Pulmonary mesenchymal stem cells are engaged in distinct steps of host response to respiratory syncytial virus infection

Melanie Brügger[1,2,3], Thomas Démoulins[1,2,§], G. Tuba Barut[1,2,3,§], Beatrice Zumkehr[1,2], Blandina I. Oliveira Esteves[1,2], Kemal Mehinagic[1,2,3], Quentin Haas[4], Aline Schögler[5], Marie-Anne Rameix-Welti[6], Jean-François Eléouët[7], Ueli Moehrlen[8], Thomas M. Marti[5,9], Ralph A. Schmid[5,9], Artur Summerfield[1,2], Horst Posthaus[2,10], Nicolas Ruggli[1,2], Sean R. R. Hall[5,9,11], and Marco P. Alves[1,2,#]

[1]Institute of Virology and Immunology, Bern, Switzerland

[2]Department of Infectious Diseases and Pathobiology, Vetsuisse Faculty, University of Bern, Bern, Switzerland

[3]Graduate School for Cellular and Biomedical Sciences, University of Bern, Bern, Switzerland

[4]Institute of Pharmacology, University of Bern, Bern, Switzerland

[5]Department of Biomedical Research, University of Bern, Bern, Switzerland

[6]Université Paris-Saclay, INSERM, Université de Versailles St. Quentin, UMR 1173 (2I), Versailles, France

[7]Université Paris-Saclay, INRAE, UVSQ, VIM, Jouy-en-Josas, France

[8]Pediatric Surgery, University Children's Hospital Zurich, Zurich, Switzerland

[9]Department of General Thoracic Surgery, Inselspital, Bern University Hospital, University of Bern, Switzerland

[10]Institute of Animal Pathology, Vetsuisse Faculty, University of Bern, Bern, Switzerland

[11]Gillies McIndoe Research Institute, Wellington, New Zealand

[§]These authors contributed equally to this work

[#]Corresponding author: marco.alves@vetsuisse.unibe.ch

Word count abstract: 154

Word count manuscript: 8170

References: 84

Figures: 6

Supporting information: 7 figures, 4 tables

ABSTRACT

Lung-resident (LR) mesenchymal stem and stromal cells (MSCs) are key elements of the alveolar niche and fundamental regulators of homeostasis and regeneration. We interrogated their function during virus-induced lung injury using the highly prevalent respiratory syncytial virus (RSV) which causes severe outcomes in infants. We applied complementary approaches with primary pediatric LR-MSCs and a state-of-the-art model of human RSV infection in lamb. Remarkably, RSV-infection of pediatric LR-MSCs led to a robust activation, characterized by a strong antiviral and pro-inflammatory phenotype combined with mediators related to T cell function. In line with this, following *in vivo* infection, RSV invades and activates LR-MSCs, resulting in the expansion of the pulmonary MSC pool. Moreover, the global transcriptional response of LR-MSCs appears to follow RSV disease, switching from an early antiviral signature to repair mechanisms including differentiation, tissue remodeling, and angiogenesis. These findings demonstrate the involvement of LR-MSCs during virus-mediated acute lung injury and may have therapeutic implications.

Keywords: mesenchymal stem and stromal cells, respiratory syncytial virus, acute lung injury, repair and regeneration, bronchiolitis, interstitial pneumonia, respiratory virus infection.

AUTHOR SUMMARY

27 This work identifies a novel function of lung-resident MSCs during virus-induced acute lung injury.
28 These findings contribute to the understanding of host response and lung repair mechanisms
29 during a highly prevalent clinical situation and may have therapeutic implications.

30

31 **INTRODUCTION**

32 The ability of organs to maintain homeostasis and regenerate following injury is vital to an
33 organism. These processes are maintained by many supportive cells including tissue-resident
34 mesenchymal stem and stromal cells (MSCs). MSCs are found in nearly every vascularized tissue
35 including the upper and lower respiratory tract. More specifically, they are localized in perivascular
36 niches of small and larger blood vessels and were shown to be lung-resident [1-7]. In the alveolar
37 niche, lung-resident (LR)-MSCs can interact with epithelial cells and promote alveolar cell growth,
38 differentiation, and self-renewal. This is of particular importance for epithelial maintenance as well
39 as for repair and regeneration as demonstrated in artificial rodent models of lung injury [8-10].
40 Failure of these mechanisms may play a role in the etiology of several chronic lung diseases [11,
41 12]. LR-MSCs can directly interact with various pulmonary immune cell populations via cellular
42 contact or in a paracrine manner by secretion of soluble factors [13]. Characterization of
43 immunomodulatory properties of mesenchymal cells are of great clinical importance since non-
44 resident MSCs are the subject of cell-based treatment approaches for various lung disorders [14,
45 15].

46 The human respiratory syncytial virus (RSV) is of high prevalence and causes a huge burden on
47 public health systems. Globally, RSV is the leading cause of severe acute lower respiratory tract
48 infections in early childhood and suspected to have an underestimated impact on the elderly [16,
49 17]. Several animal models have been established to study RSV infection, with the lamb model
50 best reflecting anatomical and immunological properties of the neonatal human lung. This model
51 recapitulates the clinical features of the human pediatric disease and the closely related bovine
52 RSV is a natural pathogen of ruminants. Furthermore, unlike rodents, lambs present a similar
53 lung development, are susceptible to human RSV, and develop comparable pulmonary lesions
54 [18-20].

55 Despite intense research on MSCs, no information is available about their role during acute
56 respiratory infection and their contribution following virus-induced injury. Given the important role
57 of the mesenchymal compartment and LR-MSCs in lung regeneration and repair, we hypothesize
58 that this applies during respiratory virus infection. Therefore, we aimed to explore the role of the

59 pulmonary mesenchymal compartment, in particular LR-MSCs, during RSV infection using an
60 experimental approach based on primary LR-MSCs isolated from human pediatric donors and a
61 translational model of human RSV infection in lamb.
62

63 ## RESULTS

64 ### LR-MSCs are highly permissive to RSV infection

65 To study the immunobiology of LR-MSCs during respiratory virus infection, we determined first if
66 these cells are susceptible towards RSV infection in comparison to a well described cellular target
67 of RSV, namely airway epithelial cells (AECs) [21-23]. We characterized the LR-MSCs isolated
68 from pediatric donors according to the three criteria proposed by the Mesenchymal and Tissue
69 Stem Cell Committee of the International Society for Cellular Therapy [24]. As shown in **Fig. 1A,**
70 LR-MSCs were positive for the three MSC surface markers CD73, CD90, and CD105.
71 Additionally, we confirmed plastic adherence of the cells and their trilineage potential by
72 differentiating them towards chondrocytes, osteocytes, and adipocytes (**Fig. 1B**). Next, we
73 assessed mRNA expression levels of different putative RSV cell-surface receptors/co-receptors
74 [25-30], namely nucleolin, toll-like receptor 4 (TLR4), intercellular adhesion molecule 1 (ICAM-1),
75 annexin II, and CX3CR1 in pediatric LR-MSCs in comparison to donor-matched AECs. All tested
76 receptors were expressed in both cell types at various levels (**Fig. 1C**), suggesting that LR-MSCs
77 are susceptible to RSV infection. Thereby, we detected fast replication kinetics of RSV RNA in
78 LR-MSCs similar to levels measured in infected AECs (**Fig. 1D**). To confirm the replication of
79 RSV in LR-MSC, we next used a flow cytometry (FCM) approach. We infected LR-MSCs with a
80 clinical isolate of RSV subtype A (RSV-ON1-H1) and with RSV-A2 at low multiplicity of infection
81 (MOI; 0.1 PFU/cell). After 144 hours post-infection (p.i.) 40-100% of LR-MSCs were infected
82 depending on the donor (**Fig. 1E**). However, when using higher MOIs (1 PFU/cell), 144 hours p.i.,
83 both RSV-A2 and RSV-ON1-H1 infected nearly 100% of the cells (**Fig. S1A**). Given that LR-
84 MSCs are highly susceptible to RSV infection, we were wondering how the virus spreads among
85 the cells. To follow visually virus spread in the two different cell types, we performed live imaging
86 in specific areas of the cellular layer following infection with a recombinant RSV construct

87 expressing constitutively the mCherry reporter (RSV-mCherry). While infected well-differentiated
88 (WD)-AECs appear as discrete RSV-positive cells, infected LR-MSCs showed up in discrete foci,
89 suggesting RSV spread via cell-to-cell contact (**Fig. 1F**). In order to confirm that the increase of
90 mCherry reporter signal in LR-MSCs foci is due to RSV spread, we infected LR-MSCs with RSV-
91 A2 and visualized the presence of RSV over time using a high definition confocal microscopy
92 approach. Notably, while the RSV signal was often located at the plasma membrane at 24h p.i, it
93 increased over time and became mainly perinuclear and/or cytosolic at later time points,
94 suggesting replication (**Fig.1G**). To further confirm the distinct life cycles, we measured infectious
95 virus release over time in LR-MSCs in comparison to WD-AECs by applying a plaque-forming
96 unit (PFU) assay. Remarkably, at most of the time-points tested, there was significantly higher
97 infectious virus release in the apical washings of infected WD-AECs compared to the
98 supernatants of LR-MSC cultures infected with a low or a high MOI. Moreover, while there was
99 almost no infectious virus detectable in the supernatants of LR-MSCs with both MOIs tested (**Fig.
100 1H, S1B**), we observed an exponential increase of the intracellular infectious RSV titers over time
101 at both MOIs tested (**Fig. 1I, S1C**). Finally, when assessing the extracellular viral RNA loads in
102 WD-AECs in comparison to LR-MSCs, we observed a rapid exponential increase of virus loads
103 in the apical washes of WD-AECs and rather an accumulation of RSV RNA in the supernatants
104 of LR-MSCs, suggesting the presence of substantial levels of non-infectious RSV particles (**Fig.
105 1J, S1D**). Altogether, these results demonstrate that primary pediatric LR-MSCs are highly
106 permissive to RSV infection and that RSV replicates in LR-MSC, although the life cycle of RSV is
107 distinct to AECs.
108

109 **RSV infection is altering the immune properties of LR-MSCs**

110 We therefore aimed to establish if LR-MSCs can mount an antiviral response upon RSV infection.
111 Twenty-four hours p.i., we observed a significant increased expression of interferon stimulated
112 genes (ISGs) commonly induced during RNA virus infections [31]. More specifically, RSV-A2 and
113 RSV-ON1-H1 infection induced a significant upregulation of retinoic acid-inducible gene-I (RIG-
114 I), melanoma differentiation-associated protein 5 (MDA-5), 2',5'-oligoadenylate synthetase 2

115 (2',5'-OAS), interferon (IFN)-induced dynamin-like GTPase (MxA), and virus inhibitory protein,
116 endoplasmic reticulum-associated, IFN-inducible (Viperin) compared to mock control (**Fig. 2A**).
117 Furthermore, the mRNA levels of both IFN-β and IFN-λ1 had a trend towards significantly higher
118 levels upon RSV infection (**Fig. 2B**). We also verified if RSV infection-induced increased mRNA
119 levels of type I and III IFNs resulted in an increased protein release. IFN-β release was
120 significantly stimulated by the two RSV strains over time and was quantified at highly significant
121 levels after 72 hours p.i. (**Fig. 2C**). Furthermore, the protein levels of IFN-λ1/3 were significantly
122 elevated after 24 and 72 hours p.i. compared to mock control for RSV-A2 and had a trend towards
123 significance for the RSV-ON1-H1 strain (**Fig. 2D**). Notably, infection of WD-AECs in comparison
124 to LR-MSCs induced comparable IFN type I and III levels 24 to 72 hours p.i., suggesting a similar
125 IFN response upon RSV infection (**Fig. S2A-C**). Next, we wanted to evaluate whether infection
126 has an impact on the immunomodulatory properties of LR-MSCs. First, we evaluated the cell-
127 surface expression levels of two co-stimulatory molecules, namely programmed death-ligand 1
128 (PD-L1) and major histocompatibility complex (MHC) class I, described in LR-MSCs to be
129 involved in their immunomodulatory characteristics [32, 33]. LR-MSCs expressed baseline levels
130 of both co-stimulators. Poly(I:C), a ligand mimicking RNA virus infection, induced a significant
131 upregulation of both co-stimulatory molecules in comparison to mock control. In line with this,
132 RSV infection led to the induction of slightly increased levels of PD-L1 and MHC class I expression
133 compared to mock-treated LR-MSCs, with differences not reaching significance, as shown in
134 representative histograms (**Fig. S2D**) and upon quantification (**Fig. S2E**). Next, we evaluated the
135 secretory profiles of LR-MSCs following RSV infection in comparison to WD-AECs. Upon infection
136 of WD-AECs with RSV-A2 or RSV-ON1-H1, the basolateral cytokine secretion revealed mainly
137 CXCL10/IP-10 and CXCL8/IL-8 release (**Fig. 2E**). Contrary to WD-AECs, RSV infection of LR-
138 MSCs led to a massive secretion of several cytokines. In fact, 24 and 72 hours p.i., expression
139 was remarkably increased for most of the cytokines measured, including CXCL10/IP-10,
140 CXCL8/IL-8, IL-6, G-CSF, CCL5/RANTES, IL-9, IFN-γ, IL-5, and L-17 to name the most notable
141 ones (**Fig. 2F**). Taken together, these data demonstrate that RSV infection leads to a robust

142 activation of LR-MSCs, characterized by a strong antiviral and pro-inflammatory phenotype
143 combined with cytokines modulating T cell function (**Fig. 2G**).
144
145 **RSV infection is causing lung injury in lamb**
146 To study the MSC compartment of the lung and its role during an acute respiratory virus infection,
147 we applied an *in vivo* approach using the neonatal lamb model of RSV infection. Although data
148 are available on ovine MSCs derived from several tissues, ovine LR-MSCs have not been
149 described yet [34-36]. Thus, we isolated and expanded LR-MSCs cultures from healthy ovine
150 lung cell suspensions as described previously for human tissue [3]. Characterization by
151 immunophenotyping displayed a high level of cell surface markers typically found in MSCs such
152 as the hyaluronate receptor CD44 and CD29 (ITGB1). An additional marker, CD166 (ALCAM),
153 was also expressed on cultured MSCs (**Fig. S3A)**. The plastic-adherent cells were large with a
154 fibroblast-like morphology. Multilineage capacity was confirmed following specific culture
155 conditions, as ovine LR-MSCs transdifferentiated to chondrocytes, osteocytes, and adipocytes
156 (**Fig. S3B**). Together, these features fulfill the accepted criteria to identify MSCs proposed by the
157 Mesenchymal and Tissue Stem Cell Committee of the International Society for Cellular Therapy
158 [24]. Before infection of the animals, we performed an infection of ovine LR-MSCs cultures with
159 human RSV. Virus replication was evident as observed by an increase of RSV load of cell-
160 associated viral RNA over time. Similarly to RSV-infected human LR-MSCs, the infectious virus
161 in the supernatants was undetectable or close to the detection limit suggesting cell-to-cell spread
162 (**Fig. S3C**). Furthermore, *ex vivo* infection of ovine precision-cut lung slice (PCLS) cultures with a
163 recombinant RSV construct expressing constitutively the green fluorescent protein (RSV-GFP)
164 led to an increase of the reporter signal over time, indicating replication (**Fig. S3D**). When
165 analyzing the infected PCLSs at higher magnification, the GFP signal was mainly located in the
166 alveolar wall suggesting infection of pneumocytes (**Fig. S3E**). Newborn lambs were infected with
167 human RSV-A2 and respiratory disease was evaluated during the acute (3 and 6 days p.i.),
168 recovery (14 days p.i.), and convalescence (42 days p.i.) phases. To do so, at each timepoint
169 p.i., we examined the lung tissue and the cellular components of bronchoalveolar lavage (BAL)

170 fluid (**Fig. 3A**). RSV-infected neonates showed clear nasal discharge, occasional coughing and
171 wheezing. Macroscopic lesions were detected at necropsies performed 3 and 6 days p.i. Lungs
172 failed to collapse and showed multiple, irregular, mildly reddened areas with slightly increased
173 consistency of up to 2 cm in diameter in all lung lobes. Histopathological evaluation of the lung
174 revealed tissue consolidation, bronchiolitis, and thickening of interalveolar walls 3, and 6 days
175 following RSV infection (**Fig. 3B**). Following infection, alveolar type 2 cell hyperplasia was
176 observed, indicating tissue injury (**Fig. S4A**). In addition, at 6 days p.i. we observed occasionally
177 potential syncytial cells lining alveoli (**Fig. S4A, B**). These features disappeared 14 days p.i. (**Fig.**
178 **3B**), indicating resolution of lesions after RSV-mediated acute lung injury. Immunohistochemistry
179 analysis of lung tissue sections revealed the presence of RSV antigen in pneumocytes (**Fig. 3C**).
180 We evaluated the viral RNA levels in the lung and BAL tissues. In the lung, the RSV loads
181 decreased over time with no virus detectable in 50% of the animals 14 days p.i. and in all animals
182 42 days p.i. In the cellular fraction of the BAL, RSV copies were highest at 3 days p.i., with viral
183 RNA detectable in 66% of the animals 14 days p.i. and reaching undetectable levels 42 days p.i.
184 There was a significant difference in viral loads with approximately 100 times higher level of RSV
185 copies detectable in the BAL compartment compared to the lung at both, 3 and 6 days p.i. (**Fig.**
186 **3D**). To confirm the histopathological evaluation revealing RSV-mediated tissue injury, we
187 assessed cell death by quantifying cleaved caspase-3-positive cells using an approach
188 summarized in **Fig. S5**. The percentage of cleaved caspase-3 positive cells in the lung, was
189 significantly increased for infected animals 3, and 6 days p.i. and similar 14, and 42 days p.i.
190 compared to mock controls (**Fig. 3E**). Lung injury is further indicated by shedding of apoptotic
191 cells into the bronchoalveolar space. Indeed, there are significantly more cleaved caspase-3
192 positive cells 3 days p.i. assessed for infected compared to mock-infected animals (**Fig. 3F**). The
193 impact of RSV infection on the bronchoalveolar space is further indicated by an infiltration of cells
194 as assessed in the BALs from infected compared to mock-infected animals 3 to 14 days p.i. (**Fig.**
195 **3G**). In summary, the life cycle of RSV is similar in human and ovine LR-MSCs and infection of
196 neonatal lambs with human RSV is causing lung injury. These data support the use of the lamb
197 model to investigate LR-MSCs in RSV disease.

198

199 **LR-MSCs are a target for RSV infection *in vivo***

200 To determine if LR-MSCs can be a target for RSV *in vivo*, we designed a FCM assay allowing the
201 identification of the pulmonary epithelial ($CD31^{-}CD45^{-}panCTK^{+}$) and mesenchymal ($CD31^{-}CD45^{-}$
202 $panCTK^{-}CD29^{+}CD44^{+}$) compartments, as well as detection of RSV infection *in vivo* (**Fig. 4A)**. In
203 13-80% of the infected animals, both RSV-positive epithelial cells and LR-MSCs were detected
204 in the lung cell suspensions 3, 6 and 14 days p.i. (**Fig. 4B, S6**). When RSV-positive LR-MSCs
205 were plotted as a function of RSV-positive epithelial cells, a significant positive association was
206 found, suggesting that the spread of RSV infection to LR-MSCs is linked to the extent of
207 replication in the pulmonary epithelium (**Fig 4C**). Next, MSCs derived from lung tissue and BALs,
208 were isolated from each animal at the different time points p.i. and expanded in culture. When
209 testing the presence of RSV within the lung-derived MSC cultures, viral RNA was detectable in
210 most cultures from the animals at 3 and 6 days p.i. and in none of the cultures isolated from
211 animals at 14 and 42 days p.i. In line with the higher viral loads in the BAL cellular fraction
212 compared to the lung tissue, we detected high levels of RSV RNA in all BAL-derived MSCs from
213 animals at 3 and 6 days p.i. and from 3 out of 7 animals isolated at 14 days p.i. RSV RNA levels
214 were undetectable in all cultures isolated from animals at 42 days p.i. (**Fig. 4D**). Interestingly, we
215 noticed giant multinucleated cells in cultures derived from infected animals which were never seen
216 for mock animal-derived cultures (**Fig. 4E**). Given that RSV spread in foci and infectious virus
217 was rarely detected in the supernatants of infected human and ovine LR-MSCs cultures, we
218 hypothesized that these phenotypically distinct cells were RSV-infected MSCs. This was
219 confirmed by confocal microscopy visualization (**Fig. 4F**) and by the infection of cultures from
220 human and ovine LR-MSCs with RSV-mCherry (**Fig. S7A, B**). Together, these results indicate
221 that the lung MSC compartment is a target for RSV infection *in vivo* during the early phase of
222 respiratory disease.

223

224 **RSV infection leads to the expansion of the pulmonary MSC niche *in vivo***

225 To investigated the impact of virus-mediate lung injury on LR-MSCs *in vivo*, we analyzed the
226 mesenchymal compartment of RSV-infected newborn lambs during the acute, recovery, and
227 convalescence phases of RSV disease. As a mild to asymptomatic RSV disease control, adult
228 animals were infected for a period of 14 days (**Fig. 5A**). Contrary to RSV-infected neonates,
229 infection of adults did not lead to any notable clinical manifestation nor macroscopic lesions, while
230 rare foci of interstitial thickening with leukocyte infiltrates and mild alveolar type 2 hyperplasia
231 were visible histologically (**Fig. 5B**). A colony-forming unit-fibroblast (CFU-F) assay was applied
232 to lung-derived cells from infected and mock-infected animals. This assay is commonly used to
233 assess the proliferative activity of MSCs and their ability to form discrete fibroblast-like colonies
234 [37, 38]. The analysis revealed a significant effect of RSV infection on the proliferative properties
235 of LR-MSCs by increasing their activity already 3 days p.i. compared to mock control (**Fig. 5C**).
236 Quantitative analysis confirmed significantly increased CFU-F counts during the acute phase of
237 infection 3 and 6 days p.i. Interestingly, there was still a nonsignificant tendency of more CFU-F
238 counts during later phases of RSV disease 14 and 42 days p.i. compared to age-matched non-
239 infected animals (**Fig. 5D**). CFU-F counts were around 20 times lower for control adults (average
240 CFU-F count of 0.6) in comparison to control neonates (average CFU-F count of 14.2), indicating
241 an age-dependent effect on the steady-state proliferative properties of LR-MSCs. However, RSV
242 infection led to a significant increase of these colonies 14 days p.i. with an average count of 6.3
243 (average CFU-F count of 29.9 for infected neonates 14 days p.i.) (**Fig. 5E, F**). These results
244 provide evidence that RSV infection leads to a stimulation of the proliferative activity and the
245 expansion of the pulmonary MSC pool, particularly in neonates compared to older animals.
246

247 **The transcriptional activity of LR-MSCs is related to the phases of RSV disease**

248 To investigate how RSV infection impacts LR-MSCs at the transcriptional level *in vivo*, we applied
249 an experimental approach developed by Spadafora *et al.*, who showed that tracheal aspirate-
250 derived MSCs retain their transcriptional signature following a short expansion in culture [39]. We
251 undertook whole transcriptome analysis from expanded LR-MSCs isolated from infected
252 neonates during the acute, recovery and convalescent phases of RSV disease in comparison to

253 mock-infected neonates. To confirm identity of MSCs expanded in culture, we calculated the
254 transcripts per million (TPM) of markers used for their identification [24, 40]. LR-MSCs had high
255 transcriptional levels of ENG (CD105), NT5E (CD73), THY1 (CD90), ITGB1 (CD29), CD44 and
256 PDGFRA among others, and lacked transcripts of HLA-DR or HLA-DQ, PTPRC (CD45), CD34,
257 ITGAM (CD11b), or PECAM (CD31) confirming their MSC identity (**Fig. 6A**). Next, we compared
258 the transcriptome profiles of LR-MSCs during the acute phase of RSV disease (6 days p.i.) to
259 mock-infected animal-derived LR-MSCs and found 14 differentially expressed genes (DEGs) to
260 be significantly upregulated. The majority of them belong to the IFN pathway and are associated
261 with antiviral responses, such as RSAD2 (Viperin), OASL, ISG15, IFI44, and IFI44L and two pro-
262 apoptotic genes, namely TNFSF10/TRAIL and STC1 (**Fig. 6B**). These findings are in line with our
263 *in vitro* results derived from human LR-MSC and support the idea that LR-MSCs mount an
264 antiviral response against RSV infection *in vivo*. Remarkably, while there was no significant
265 difference in the recovery phase (14 days p.i.) compared to mock-infected control (**Fig. 6C**), there
266 were 43 DEGs differentially expressed in LR-MSCs isolated during the convalescence phase (42
267 days p.i.) (**Fig. 6D**). Several of these genes are associated with secretory pathway, including
268 MAGE2 (protein trafficking), TBC1D20 (autophagosome maturation), MAP7D3 (microtubule
269 assembly), and MARCHF9 (protein processing). In line with this, high transcriptional activity of
270 LR-MSCs during the convalescence phase is evidenced by the upregulation of various non-
271 coding RNAs and ribonuclease proteins involved in pre-RNA processing and regulation of
272 transcription and/or translation. Furthermore, genes linked with differentiation and developmental
273 processes, such as SOX4 NOC3L, and C2CD3 were differentially expressed during the
274 convalescence phase. Remarkably, many of the upregulated DEGs were related to endothelial
275 cell function and angiogenesis, such as TRPC4 or KDR which codes for the vascular endothelial
276 growth factor receptor 2 (VEGFR2), and ITGA9, the receptor of VCAM1. Finally, among the top
277 downregulated DEGs were two genes coding for matrix-metalloproteases (MMPs), MMP1 and
278 MMP3, which are involved in the remodeling of the extracellular matrix (ECM). The list of
279 significant DEGs and associated literature from infected *versus* noninfected animal-derived LR-
280 MSCs is provided in **Table S1.** To confirm the interpretation of our findings, we used a

281 computational method for pathway enrichment analysis of the transcriptional profiles of LR-MSCs
282 over RSV infection. Gene set enrichment analysis (GSEA) revealed that the transcriptional
283 signature of LR-MSCs isolated from RSV- and mock-infected animals is retained during the short
284 *ex vivo* culture phase and is following the different phases of respiratory disease. During the acute
285 phase of infection, the significant enriched hallmark gene sets were associated to IFN pathway,
286 inflammation, and stress response. Notably, the only enriched gene set downregulated in the
287 acute phase of RSV infection was Notch signaling, a central pathway regulating cell proliferation
288 and differentiation. During the recovery and the convalescence phases, shared gene sets
289 associated with cell cycle regulation, such as E2F and Myc pathway, were downregulated
290 compared to mock controls. Further, during the convalescence phase of RSV disease, five
291 additional hallmark gene sets were upregulated. More precisely, the transcriptional signature of
292 LR-MSCs isolated from infected animals long after viral clearance revealed processes such as
293 myogenesis, epithelial-mesenchymal transition (EMT), angiogenesis, p53 pathway, and TGF-β
294 signaling, suggesting that LR-MSCs are involved in tissue repair and regeneration following virus-
295 induced injury (**Fig. 6E**). To sum up, these results show that LR-MSCs, are activated during virus-
296 induced lung injury by an increase in their proliferative activity and by mounting dynamic
297 transcriptional profiles leading to an early antiviral and inflammatory response followed by
298 mechanisms associated with tissue remodeling, repair and regeneration (**Fig. 6F**).
299

300 **DISCUSSION**

301 This work was undertaken to explore the role of the pulmonary MSC compartment during acute
302 respiratory virus infection and its contribution to lung repair. Our investigations herein reveal upon
303 infection, LR-MSCs mount an antiviral response and release a variety of immunomodulatory
304 mediators, which may have a biological impact on the pulmonary microenvironment. Furthermore,
305 we show that RSV-mediated lung injury activates and stimulates the expansion of LR-MSCs
306 which mount a dynamic transcriptional program related to mechanisms of repair and
307 regeneration.

308 Contrary to the well-described replication of RSV in AECs, the primary cellular target of RSV
309 infection [21-23], our data indicates a distinct life cycle in LR-MSCs with viral spread via cell-to-
310 cell contact. Such mechanism may improve virus dissemination and promote immune evasion
311 [41]. In a humanized mouse model, pulmonary mesenchymal cells were shown to be susceptible
312 to different viruses such as Middle East respiratory syndrome coronavirus, Zika virus, and
313 cytomegalovirus [42]. In addition, they were recently proposed as an immune-privileged niche for
314 *M. tuberculosis* persistence [43]. Since LR-MSCs are described to localize perivascular and in
315 close proximity to the respiratory and alveolar epitheliums, this makes them a potential
316 nonepithelial target for virus infection. Here, we show accessibility of LR-MSCs possibly through
317 physical disruption of the alveolar epithelium. Indeed, already 3 days p.i., we observed evidence
318 of lung injury associated with alveolar infection and concomitant LR-MSCs targeting by the virus.
319 RSV infections can lead to a number of extrapulmonary manifestations [44]. Assuming the
320 presence of MSCs in most tissues, it is conceivable that in some predisposed subjects, RSV may
321 target other MSC niches throughout the body. In line with this, bone marrow and umbilical cord
322 vein MSCs were shown to be susceptible to RSV infection *in vitro* [45, 46].
323 During the acute phase of RSV disease, we observed RSV-positive multinucleated LR-MSCs in
324 the BAL-expanded cultures, indicative of a cytopathic effect on these cells. Thereby, the
325 concomitant expansion of the pulmonary MSC compartment is potentially indicative of a
326 replenishment of the lost fraction of LR-MSCs following RSV infection. Furthermore, we show that
327 RSV infection is signaled by LR-MSCs through the induction of antiviral and pro-inflammatory
328 mediators, both associated with RSV disease severity [47-49]. In addition, RSV infection of LR-
329 MSCs lead to a type I and III IFN release and subsequent ISGs induction, shifting LR-MSCs
330 towards an antiviral state. This is in line with the pro-inflammatory and antiviral transcriptional
331 signatures found in LR-MSCs, isolated form infected animals during the acute phase of RSV
332 disease. In mice, it has been shown that IFN signaling of the lung stromal compartment was
333 protective against influenza virus by reducing viral replication [50]. Massive lung infiltration of
334 immune cells following cytokine release, termed “cytokine storm”, is characteristic of severe
335 respiratory virus infections including RSV [51]. Among the most abundant chemokines in infants

336 suffering from RSV bronchiolitis are CXCL10/IP-10, CXCL8/IL-8, CCL2/MCP-1 and CCL3/MIP-
337 1α. Similarly, in our setting, RSV infection of LR-MSCs led to a massive release of chemokines
338 with the potential to attract neutrophils, eosinophils, monocytes, and lymphocytes, such as
339 CXCL8/IL-8, CCL5/RANTES, CCL2/MCP-1, and CXCL10/IP-10, respectively. In RSV disease, it
340 is believed that the cellular sources of the pulmonary chemokine responses are epithelial and
341 inflammatory immune cells; our data suggests that LR-MSCs might provide an additional source
342 [52].
343 Besides the vast chemokine production, RSV infection of LR-MSCs led as well to the release of
344 a number of other mediators and growth factors. Interestingly, the secretory profile of RSV-
345 infected LR-MSCs was very distinct to the one described for RSV infected BM-MSCs, supporting
346 tissue specificity of MSC populations [45, 53, 54]. Notably, VEGF, a key mediator of angiogenesis,
347 is released by pediatric LR-MSCs at increased levels after RSV infection. Also, the transcriptional
348 profiles of LR-MSCs isolated during the convalescence phase of RSV disease were related to
349 endothelial biology and pathway analysis revealed pro-angiogenic enriched gene sets. In line with
350 this, using an adult rat model, VEGF signaling disruption was shown to cause an enlargement of
351 the air spaces and an alteration of the alveolar structure, suggesting that VEGF has a crucial role
352 during normal adult alveolarization [55]. Considering the perivascular location of MSCs in tissues,
353 our data indicate that LR-MSCs may modulate endothelial cells activity during virus-induced lung
354 injury.
355 TGF-β is a central regulator of the respiratory system and controls epithelial and mesenchymal
356 cell fate through several mechanisms such as promotion of EMT, myofibroblast differentiation,
357 and stimulation of ECM production and remodeling [56]. Our transcriptional data from LR-MSCs
358 isolated from infected animals during the convalescence phase of RSV disease, revealed that
359 these cells might play a role in these mechanisms. Indeed, compared to noninfected control-
360 derived LR-MSCs, their transcriptome profiles are linked with TGF-β signaling and EMT. The
361 latter is linked with the acquisition of more proliferative stem-like states providing an additional
362 link between activation of EMT and wound healing [57]. In line with this, the p53 pathway
363 activation further supports the maintenance of MSC stemness for subsequent repair processes

364 [58]. Transcriptome analysis of LR-MSCs isolated long after virus clearance, positively associated
365 with myogenesis. Myofibroblasts, an activated type of mesenchymal cells and an important
366 source of ECM, participates in tissue repair but their persistence after wound healing is linked to
367 fibrotic disorders [59]. Thus, failure of these mechanisms may potentially increase the risk of
368 developing fibrotic abnormalities following respiratory virus infections. Comorbidities such as
369 recurrent wheezing and asthma are happening years after RSV infection has resolved. To date,
370 it remains unclear if pulmonary mesenchymal cells deficiency in lung repair and regeneration are
371 linked with such disorders [60, 61].
372 Due to their immunomodulatory properties, MSCs are applied in cell-based therapies with
373 promising outcomes for the treatment of pulmonary morbidities such as idiopathic pulmonary
374 fibrosis (IPF), acute-respiratory distress syndrome (ARDS) and severe influenza infections [14,
375 62-65]. Furthermore, the current coronavirus disease 2019 (COVID-19) pandemic is leading to a
376 strong interest in MSCs as a treatment option for severe COVID-19 cases. As a consequence,
377 an increasing number of clinical investigations of such MSC-based therapy approaches are under
378 evaluation [66-69]. Safety concerns regarding susceptibility of MSCs towards different viruses, as
379 well as potential viral reactivation events have been raised [70]. On one hand, our data indicate
380 eventual safety concerns due to the targeting of LR-MSCs during the acute phase of virus
381 infection. On the other hand, we provide evidence that LR-MSC seem to have a beneficial effect
382 after virus clearance, supporting the use of MSC-based therapies to treat virus-induced lung
383 injury.
384 The ovine lung is a classical model of the human respiratory tract due to similarities in size,
385 structure, development and immune system [71]. However, some limitations should be
386 mentioned. First, we observed a high animal-to-animal variability in most endpoints measured,
387 probably due to the outbred nature of the animals. While this might look like a limitation, we believe
388 it reflects best the situation in humans compared to inbred models. Secondly, we used the isolated
389 LR-MSCs as a single population but previous single-cell transcriptomic studies demonstrated that
390 MSC, are a rather heterogeneous population composed of distinct MSC subsets [8, 9, 72]. Third,
391 due to the lung size, we analyzed three pooled specimens, representative of each lung region.

392 This might explain why we didn't detect RSV-positive cells for some animals for whom productive
393 infection was demonstrated by the assessment of the viral loads.
394 In summary, our data demonstrate the involvement of pulmonary MSCs during respiratory virus
395 infection. While being a target for RSV, these cells can respond to infection by switching to an
396 antiviral state and by a profound remodeling of their immune phenotype. Furthermore, LR-MSCs
397 show hallmarks of tissue repair and regeneration processes after viral clearance. Our findings
398 identify a function of LR-MSCs in a highly prevalent clinical situation and constitute a basis for
399 further exploration of the pulmonary mesenchymal compartment during respiratory viral
400 infections.
401

402 ## MATERIAL AND METHODS

403 **Virus propagation and titration**

404 Human RSV-A2 strain was derived from ATCC (VR-1540, GenBank accession number
405 KT992094.1). The recombinant RSV-mCherry is described elsewhere [73] and the RSV-GFP
406 construct was generated by Mark Peeples (Nationwide Children's Hospital Columbus, USA) [74]
407 and kindly provided by Dominique Garcin (University of Geneva, Switzerland). The clinical RSV
408 isolate, RSV-ON1-H1, was collected from a child below the age of five years with confirmed RSV
409 infection, hospitalized at Hannover Medical School, Germany. The virus was isolated from
410 nasopharyngeal aspirates and was passaged up to five times in HEp-2 cells (ATCC, CCL-23).
411 The caregivers gave informed consent for the donation of nasopharyngeal aspirates, and all steps
412 were conducted in compliance with good clinical and ethical practice and approved by the local
413 ethical committee at Hannover Medical School, Germany (permission number 63090/2012) [75].
414 All RSV strains were propagated on HEp-2 cells, cultivated in DMEM (Gibco) supplemented with
415 10% fetal bovine serum (FBS, Gibco). Briefly, HEp-2 cells were infected at a MOI of 0.02 PFU/cell
416 for 2 hours before the addition of DMEM supplemented with 5% FBS. The cell-associated virus
417 was harvested by scraping the cell monolayer when 60% of cytopathic effect was observed. The
418 virus was released from the cells by one freeze-thaw cycle followed by centrifugation to get rid of
419 cell debris. Virus stocks were stored in aliquots containing 10% sucrose (Sigma) at -150°C. To

420 prepare a mock control the same procedure was applied without adding virus. A similar approach
421 was applied to assess the intracellular RSV titers from infected LR-MSCs. For virus titration, serial
422 dilutions of supernatants were added to HEp-2 cells and incubated for 48-96 h at 37°C, 5 % CO_2.
423 Next, the cells were washed with PBS, fixed with methanol supplemented with 2% H_2O_2 and
424 incubated with a biotinylated anti-RSV antibody (Bio-Rad) in PBS containing 1% bovine serum
425 albumin (BSA, Sigma) for 1 h, followed by 30 min incubation with ExtrAvidin Peroxidase (Sigma)
426 and staining with 3,3′-diaminobenzidine substrate (Sigma). Virus titers were expressed as
427 PFU/ml.
428
429 **Primary cells**
430 Primary pediatric MSCs were obtained as described previously [32, 72]. Briefly, healthy lung
431 tissue was obtained from pediatric patients undergoing elective surgery for congenital pulmonary
432 airway malformation and other various airway abnormalities at the Children's University Hospital
433 of Zurich (n=9, age range: 5 days to 181 months, (**Table S2**)). Written informed consent was
434 obtained for all the patients and/or parent/guardian and the study protocol was approved by the
435 local Ethics Commission of the Canton of Bern (KEK-BE:042/2015). Minced tissue was further
436 disaggregated enzymatically using a solution containing collagenase I and II (Worthington
437 Biochemicals) at a concentration of 0.1 and 0.25%, respectively. Further, digestion buffer was
438 supplemented with 0.2 mg/ml deoxyribonuclease I (Biochemicals) to the digestion buffer to
439 prevent cell clumps and improve cell recovery. To isolate MSCs, a FCM assay was applied using
440 a panel of fluorescently-conjugated human monoclonal antibodies: CD45, CD14, CD31, and
441 EpCAM for negative and CD73 and CD90 for positive selection. FACS-sorted MSCs were
442 expanded in tissue culture flasks pre-coated with 0.2% gelatin solution (Sigma) and in chemically
443 defined growth medium consisting of α-MEM with ribonucleosides (Sigma) supplemented with
444 1% FBS, GlutaMAX (Invitrogen), 10 ng/ml of recombinant human fibroblast growth factor 2 (FGF2,
445 Life Technologies), 20 ng/ml of recombinant human epidermal growth factor (EGF, Life
446 Technologies), human insulin (Sigma), 10'000 units/ml of penicillin and 10'000 µg/ml streptomycin
447 (Sigma). Cells were maintained in a humidified atmosphere at 37°C, 5% CO_2 until confluence was

448 reached. The medium was aspirated carefully and replaced with fresh medium six days after
449 plating and after that point performed twice a week. Cells were used prior to passage 5 in all
450 experiments. WD-AECs isolated from independent healthy donors (MucilAir™, Epithelix Sàrl,
451 Geneva, Switzerland) were used for RSV infection. The cultures were maintained on 24-well
452 transwell inserts (Corning) at the air-liquid interface (ALI) in MucilAir™ culture medium (Epithelix
453 Sàrl, Geneva, Switzerland) in a humidified incubator at 37° C, 5% CO_2. Every 3 days culture
454 medium was changed. The apical surface was rinsed with Hank's balanced salt solution (HBSS,
455 ThermoFisher) once a week and prior to infection, to washout the mucus.
456
457 **Precision-cut lung slices**
458 Isolated ovine lungs were infused with 1.5% low-melting point agarose (Promega) in DMEM and
459 subsequently put into cold PBS in order to allow the agarose to solidify. Next, the perfused lung
460 tissue was cut into pieces of 0.1-1 cm^3 and embedded in 4% low-melting point agarose. An
461 automated vibrating microtome (VT1200S, Leica Biosystems) was used at a speed of 0.1 mm/sec
462 and an amplitude of 2.5-2.8 to generate PCLS with a thickness of 200 µm. Uniformly sized slices
463 were punched at a diameter of 8.5 mm. The PCLS were maintained in DMEM, supplemented with
464 1% FBS, 10'000 units/ml of penicillin and 10'000 µg/ml streptomycin, and Amphotericin B (all from
465 ThermoFisher) in a humidified atmosphere at 37°C, 5% CO_2. The culture medium was changed
466 every 24 h and the PCLS cultures were infected 2-3 days following preparation.
467
468 **RSV infection**
469 To perform infection of primary pediatric LR-MSCs and AECs with RSV-A2, RSV-mCherry, or
470 RSV-ON1-H1, 10^5 cells per well of a 12 well plate were seeded 24 h prior to infection and/or
471 stimulation. Cells were infected at selected MOIs of RSV or mock-control in FBS-free medium for
472 1 h at 37°C and 5% CO_2. Subsequently, cells were washed three times with 1X PBS and then
473 incubated in growth medium. Ten µg/ml of poly(I:C) (Sigma) was applied in growth medium and
474 incubated alike until harvesting. At selected time points, supernatants and cells were harvested
475 and stored appropriately for further analysis. For infection of WD-AECs, virus preparations were

476 diluted in medium and virus dilutions were applied apically to the tissue, assuming an average of
477 500,000 cells per insert. As a mock control, the culture supernatant of mock-infected HEp-2 cells
478 was used. Virus particles were allowed to adsorb for 3 h at 37°C and 5% CO_2 before the inoculum
479 was removed and each insert was carefully washed three times with pre-warmed HBSS and
480 placed on a new well containing fresh MucilAir™ culture medium. For stimulation of the WD-AEC
481 inserts, 10 µg/ml poly(I:C) were applied to the basolateral chamber containing the culture medium.
482 For examination of infectious viral particle release 2, 24, 48, 72, and 144 hours p.i., 250 µl HBSS
483 was added to the apical surface and incubated for 20 min at 37°C, harvested, and stored at −70°C
484 until further analysis. Basolateral media was collected and similarly stored, and replaced with
485 fresh media in the basolateral chamber of the inserts. For the infection of ovine PCLS, $5x10^5$ PFU
486 of RSV-GFP per PCLS were applied in growth medium, supplemented with 0.1% FBS and
487 incubated for 24 h at 37°C and 5% CO_2. Subsequently, the infection medium was changed to
488 growth medium and media was changed every 24 h.
489
490 **RNA isolation and quantitative PCR**
491 Total RNA of primary pediatric LR-MSCs, human AECs, and ovine lung- and BAL-derived cultured
492 MSCs was extracted using the Nucleospin RNA Plus Kit (Macherey-Nagel) according to the
493 manufacturer's protocol. For the isolation of the total RNA from the supernatants of infected LR-
494 MSCs, we used the QIAamp Viral RNA kit following manufactures recommendations (Qiagen).
495 For reverse transcription and synthesis of complementary DNA the Omniscript RT Kit (Qiagen)
496 using random hexamers (Invitrogen) was applied. Quantitative PCR was performed with target-
497 specific primers using the TaqMan Gene Expression Assay (Applied Biosystems) or the Fast
498 SYBR Green Assay (ThermoFisher) on an ABI Fast 7500 Sequence Detection System (Applied
499 Biosystems). For lung tissue and the BAL cellular fraction quantification was performed using
500 AgPath-ID™ One-Step RT-PCR Reagents (ThermoFisher), according to the manufacturer's
501 instructions. The data were analyzed using the SDS software (Applied Biosystems). Relative
502 expression was calculated with the ΔΔCT method [76]. The expression levels of the genes of
503 interest, were normalized to the housekeeping 18S rRNA. For the analysis of viral loads, RNA

504 copy numbers were interpolated from a standard curve generated with the serial dilution of a
505 plasmid containing the cDNA of the RSV L gene or the housekeeping 18S rRNA. The sequence
506 of all the primers and probes is summarized in **Table S3**.
507
508 **Flow cytometry**
509 FCM assays using different multicolor staining protocols were applied for the analysis of co-
510 stimulatory molecule expression and RSV infection of primary pediatric LR-MSCs, for the
511 identification and analysis of RSV infection of different cell types (AECs and LR-MSCs) in lung
512 cell suspensions derived from lambs, the assessment of apoptosis in the lung and the alveolar
513 space of infected and mock-infected animals. Further, a combination staining was applied to
514 evaluate the phenotype of cultured LR-MSCs. The detailed list of reagents used is summarized
515 in **Table S4**. FCM acquisitions were performed using a BD FACS Canto II (BD Bioscience) using
516 the DIVA software and were further analysed with the FlowJo software version 10.6.0 (BD). Dead
517 cells were excluded by electronic gating in forward/side scatter plots, followed by exclusion of
518 doublets as well as LIVE/DEAD® Fixable Dead Cell Staining (Invitrogen). Permeabilization and
519 fixation were undertaken according to the manufacturer's protocol (BD and Invitrogen).
520
521 **Trans-differentiation assay**
522 For differentiation, pediatric LR-MSCs (passage 5) and ovine LR-MSCs (passage 3) were plated
523 in a 24-well plate in regular culture medium and placed in a humidified atmosphere at 37°C with
524 5% CO_2. After 48 hours, cells were washed with PBS and complete differentiation media of the
525 different StemPro Differentiation Kits (Thermofisher) was added. For adipogenic induction cells
526 were plated at 10^4 cells/cm^2, for chondrogenic induction cells were plated at 2.7×10^4 cells/cm^2,
527 and to induce osteogenic differentiation, cells were plated at 5×10^3 cells/cm^2. Medium was
528 changed twice a week and after 15-21 days, cells were fixed with 4% PFA (Sigma). Adipocytes
529 were stained with Oil Red O (Sigma) to detect the formation of lipid droplets and counterstained
530 with hematoxylin (Carl Roth). Chondrocytes were stained with Alcian Blue (Sigma) to visualize

531 glycosaminoglycan synthesis and Alizarin Red S staining (Sigma) was used to detect Ca^{2+}
532 deposits in osteocytes.
533
534 **Microscopy analysis**
535 Ovine BAL-derived MSCs and culture expanded pediatric LR-MSCs were cultured on a Nunc™
536 Lab-Tek™ II Chamber Slide™ System with 50'000 cells per chamber (ThermoFisher). Next, the
537 cells were washed with cold PBS with Ca^{2+} and incubated with Wheat Germ Agglutinin (WGA)-
538 AF633 (Molecular Probes) for 10 min at 4°C. Then, cells were fixed with 4% PFA for 10 min at
539 room temperature. Next, the cells were washed with 0.3% saponin (Sigma) and stained with RSV-
540 fusion protein antibody (Millipore) for 20 min at 4°C. Then, 20 min incubation at 4°C with anti-
541 mouse IgG2a-AF546 or -AF488 (both ThermoFisher) was applied. Finally, DAPI (Sigma) was
542 added for 5 min at 37°C and cells were washed three times with cold PBS with Ca^{2+} before
543 mounting with MOWIOL® 4-88 Reagent (Sigma-Aldrich). The detailed list of antibodies used is
544 summarized in **Table S4**. Confocal microscopy analysis was performed with a Nikon Eclipse Ti
545 microscope (Nikon). All images were acquired using a 63X oil-immersion or a 40X objective. The
546 images were analyzed with IMARIS 7.7 software (Bitplane) with threshold subtraction and gamma
547 correction. To monitor the spread of RSV-mCherry infection in WD-AEC in comparison to MSC
548 cultures, a Nikon BioStation CT was used (Nikon). The cultures were followed over a period of 2
549 days with a 10X objective and images were acquired in an automated sequence every 4 to 8
550 hours following infection. Reporter expression of RSV-mCherry-infected pediatric LR-MSCs,
551 ovine LR-MSCs, and RSV-GFP-infected ovine PCLS was assessed using an Evos FL Auto 2 cell
552 imaging system (ThermoFisher) or a Leica TCS-SL, respectively. The micrographs from the trans-
553 differentiation assays were captured using an inverted microscope ECLIPSE TS100 with a Nikon
554 DS-Fi3 camera using a DS-L4 application v.1.5.03 (all form Nikon).
555
556 **Immunoassays**
557 When performing cytokine quantification, the supernatants and the basolateral medium from
558 RSV-A2 and RSV-ON1-H1 infections as well as of poly(I:C)-stimulated and unstimulated, and

559 mock-infected pediatric LR-MSCs and WD-AECs, respectively, were harvested after 24 and 72 h
560 of culture at 37°C with 5% CO_2. Human IFN-β, IFN-λ1/3 concentrations were determined using
561 commercial enzyme-linked immunosorbent assay (ELISA) kits (R&D Systems) following the
562 manufacturer's protocol. For the multiplex assay, the Pro™ Human Cytokine 27-plex Assay (Bio-
563 Rad) was used according to the manufacturer's protocol and read on a Bio-Plex 3D suspension
564 array system including a Bio-Plex Manager software v 6.0 (Bio-Rad).
565
566 **Animals**
567 The experiments with lambs were performed in compliance with the Swiss animal protection law
568 (TSchV SR 455.1; TVV SR 455.163). They were reviewed by the cantonal committee on animal
569 experiments of the canton of Bern, Switzerland and approved by the cantonal veterinary authority
570 with the license number BE125/17 (Amt für Landwirtschaft und Natur LANAT, Veterinärdienst
571 VeD, Bern, Switzerland). Newborn lambs, males and females were allocated randomly to different
572 groups (see below). Before and during the experiment, they were kept with their ewes. In order
573 to prevent secondary bacterial infections, the lambs received a prophylactic long-acting antibiotic
574 treatment by intramuscular injection of an oxytetracycline hydrochloride preparation (Cyclosol LA,
575 20 mg/kg) starting at 18 to 24 h before RSV infection. The treatment was repeated 2 times with 4
576 days interval. The trans-tracheal RSV inoculation was performed under sedation and analgesia
577 by intramuscular injection of a mixture of midazolam (Dormicum) 0.2 mg/kg and butorphanol
578 (Morphasol) 0.2 mg/kg. The trachea was punctured between the tracheal rings with a 0.9 x 40
579 mm needle (20G) and a volume of 2 ml of virus (10^8 PFU) or PBS (mock-infected controls) were
580 injected. Body temperature, body weight and clinical status (respiratory and heart rates) were
581 assessed daily by a veterinarian, whenever possible by the same person to ensure unbiased
582 clinical assessment. At defined time points, namely at 3, 6, 14, and 42 days p.i., the lambs were
583 euthanized and examined for gross- and histopathology. The lung was processed for *post-*
584 *mortem* bronchoalveolar lavage.
585
586 **Histopathological evaluation of lung tissue**

587 Lung specimens were fixed in 4% buffered formalin for 48 h, embedded in paraffin and routinely
588 processed for histology. Histological sections of 3 μm were stained with hematoxylin and eosin
589 coloration and observed by light microscopy. For immunohistochemistry, deparaffinization of the
590 sections was done with xylol for 5 minutes followed by rehydration in descending concentrations
591 of ethanol (100, 95, 80, and 75%). H_2O_2 (3.25% in methanol, 10 min at room temperature)
592 inhibited endogenous peroxidase activity. Then, the slides were incubated in boiling citrate buffer
593 (pH 6.0) for 10 min for antigen retrieval. 1% BSA (10 min) was used for blocking of nonspecific
594 antibody binding, followed by an overnight incubation at 4°C with the primary antibody targeting
595 RSV (ThermoFisher). For secondary antibody incubation and signal detection LSAB and AEC
596 Kits (DakoCytomation) were used following the manufacturers protocol. Counterstaining was
597 done with Ehrlich hematoxylin and cover slips were mounted using Aquatex (Merck) [77].
598
599 **Processing of lung tissue and bronchoalveolar lavage**
600 One specimen per lung region (cranial, middle, and caudal) were pooled and dissociation was
601 done using a collagenase I and II and a DNase I enzyme mix (all from BioConcept) and the
602 gentleMACS Octo Dissociator (Miltenyi Biotec). Following this mechanical and enzymatical
603 dissociation, the samples were applied to a sieve, to remove any remaining particulate matter.
604 The cell suspensions were passed through cell strainers (100 and 70 µm pore-size, Falcon) and
605 centrifuged at 350g for 10 min at 4°C to obtain single-cell suspensions. For the isolation of cells
606 from BALs, the lungs were isolated with the trachea, which was clamped before cutting, to prevent
607 blood from entering the lungs. Then, a PBS-containing antibiotic solution with 100 units/ml of
608 penicillin and 100 µg/ml streptomycin (both Sigma), and 2.5 μg/ml Amphotericin B was poured
609 into the lungs through a sterile funnel (200-500 ml). The cell suspensions were then passed
610 through cell strainers (100 and 70 µm pore-size, Falcon) and centrifuged at 350g for 10 min at
611 4°C to obtain single cell suspensions. If needed, red blood cells were lysed by resuspending the
612 pellet with 2 ml of H_2O and washed immediately in cold PBS before centrifugation at 350g for 10
613 min at 4°C. Cells were then processed for FCM analysis, CFU-F assay or expanded in culture to
614 obtain lung-derived MSCs. To isolate and expand MSCs in culture, lung cell suspensions were

615 seeded at a density of $3.5x10^4$ cells per cm^2 in tissue culture flasks as described previously [3].
616 Cells were maintained in α-MEM (Thermofisher) supplemented with 10% FBS (ThermoFisher),
617 an antibiotic solution containing 100 units/ml of penicillin and 100 µg/ml streptomycin, and 2.5
618 µg/ml Amphotericin B. After one to two days, the medium was changed and cells were maintained
619 at 37°C with 5% CO_2 until reaching ~80% of confluence. Regular media changes were performed
620 twice a week.
621
622 **Colony-forming unit-fibroblast assay**
623 Lung single-cell suspensions were seeded at a density of $3.5x10^4$ cells per cm^2 in a six-well plate
624 as described previously [3]. Cells were fixed after 7-14 days with ice-cold methanol for 20 min
625 and then washed with PBS. The cells were stained with Giemsa stain for 6 min, rinsed with H_2O,
626 and air-dried. Images were captured using an ImmunoSpot analyzer (CTL). Two experienced
627 investigators performed the CFU-F counts independently.
628
629 **RNA isolation and mRNA sequencing and data analysis**
630 For mRNA sequencing, total RNA was extracted from ovine LR-MSCs using TRIzol reagent
631 (ThermoFisher) in combination with the Nucleospin RNA Kit (Machery-Nagel) as previously
632 described [78]. In short, cells were lysed with 1 ml of TRIzol reagent and kept at -70°C until further
633 processing. After thawing, 0.2 ml chloroform was added to the TRIzol lysate and the samples
634 were mixed vigorously and incubated for 2-3 min at room temperature. The extractions were then
635 centrifuged at 12'000g for 15 min at 4°C. The aqueous phase was collected and mixed with 500
636 µl 75% ethanol and the RNA precipitated for 10 min at room temperature. The RNA precipitate
637 was further purified with the Nucleospin RNA kit according to the manufacturer's instructions. The
638 quantity and quality of the extracted RNA was assessed using a ThermoFisher Scientific Qubit 4.0
639 fluorometer with the Qubit RNA BR Assay Kit (Thermo Fisher Scientific) and an Advanced Analytical
640 Fragment Analyzer System using a Fragment Analyzer RNA Kit (Agilent), respectively. Thereafter, cDNA
641 libraries were generated using an illumina TruSeq Stranded mRNA Library Prep (illumina) in combination
642 with IDT for Illumina – TruSeq RNA UD Indexes (Illumina). The illumina protocol was followed using the

643 recommended input and quality of total RNA. The quantity and quality of the generated NGS libraries were
644 evaluated using a Thermo Fisher Scientific Qubit 4.0 fluorometer with the Qubit dsDNA HS Assay Kit
645 (ThermoFisher) and an Advanced Analytical Fragment Analyzer System using a Fragment Analyzer NGS
646 Fragment Kit (Agilent), respectively. The library pool was paired end sequenced using a NovaSeq 6000 SP
647 Reagent Kit v1.0, 100 cycles (illumina) on an Illumina NovaSeq 6000 instrument. The quality of the
648 sequencing runs was assessed using illumina Sequencing Analysis Viewer (illumina version 2.4.7) and all
649 base call files were demultiplexed and converted into FASTQ files using illumina bcl2fastq conversion
650 software v2.20. The average number of reads per library was 33.5 million. The RNA quality-control
651 assessments, generation of libraries and sequencing runs were performed at the Next Generation
652 Sequencing Platform, University of Bern, Switzerland. Analysis of the RNA-seq data was performed
653 at the Interfaculty Bioinformatics Unit at the University of Bern, Switzerland. RNAseq data quality
654 was assessed using fastqc v. 0.11.5 and RSeQC v. 2.6.4 [79]. The reads were mapped to the
655 *Ovis aries* reference genome (Oar_v3.1) with Hisat2 v.2.1.0 [80]. To count the number of reads
656 overlapping with each gene, as specified in the Ensembl annotation FeatureCounts from Subread
657 v.1.5.3 [81] was used. The Bioconductor package DESeq2 [82] was applied to test for differential
658 gene expression between the experimental groups. To evaluate gene expression levels of MSC
659 markers we applied the TPM normalization method [83]. The molecular signatures database
660 (MSigDB) with the Hallmark gene sets was used for gene set enrichment analysis (GSEA) [84].
661 Analysis was done using R v.3.4.4 (2018-03-15).
662
663 **Statistical analysis**
664 The Prism 8 software (GraphPad) was used for statistical analysis. To determine differences
665 between two groups, non-parametric paired Wilcoxon test or Mann–Whitney U-test were used.
666 For multiple comparisons one-way ANOVA with Tukey post-hoc test or Kruskal-Wallis test with
667 Dunn's correction were used. A $p < 0.05$ was considered statistically significant.
668
669 **NOTES**
670 **Acknowledgment**

671 We are grateful to Sylvie Python and Aurélie Godel for technical assistance; Inês Margarida
672 Berenguer Veiga, Nathan Leborgne, Loic Borcard, Amal Fahmi and Charaf Benarafa for
673 participation in the animal trial; Hans-Peter Lüthi, Roman Troxler, Jan Salchli, Daniel Brechbühl,
674 Katarzyna Sliz, and Veronika Ayala for animal care. We thank Dominic Garcin for sharing the
675 RSV-mCherry construct and Mark E. Peeples for the RSV-GFP construct. We thank Sibylle Haid,
676 Martin Wetzke, Gesine Hansen, and Thomas Pietschmann for sharing the RSV-ON1-H1 isolate.
677 We thank Heidi Tschanz-Lischer, Irene Keller, and Jenna Kelly for their bioinformatics support.
678 We thank Christoph Aebi for helpful discussions. We thank all study participants and their families.
679 This work was supported by grants from the Swiss National Science Foundation (project No.
680 310030_172895) and from the Bangerter-Rhyner Foundation (both to MPA).
681

682 **Competing interest**

683 All the authors declare that they have no competing interests.

684

685 **Data availability statement**

686 The data generated and analyzed during the current study are available from the corresponding
687 author on reasonable request.

688

689 **Author's contributions**

690 Conception and design: MPA, MB. Collection of pediatric samples: UM, TMM, RAS, SRRH.
691 Acquisition of data: MB, BZ, TD, KM, NR, BIOE, QH, AS, SRRH. Contribution to reagents: MARW,
692 JFE. Analysis and interpretation: MPA, MB, KM, HP, GTB. Drafting the manuscript: MB, MPA.
693 Final approval of the manuscript: all authors.

694

695 **SUPPORTING INFORMATION**

696 Figure S1. Infection of LR-MSCs with RSV at a MOI of 1 PFU/cell

697 Figure S2. IFN mRNA levels and PD-L1 and MHC class I surface expression in RSV-infected LR-
698 MSCs
699 Figure S3. RSV-infection of ovine PCLS and ovine LR-MSCs
700 Figure S4. Presence of syncytium in neonatal lungs following RSV infection
701 Figure S5. FCM assay for apoptosis detection *in vivo*
702 Figure S6. Targeting of AECs and LR-MSCs following neonatal RSV infection
703 Figure S7. Formation of syncytium upon RSV infection of human and ovine LR-MSCs
704 Table S1. List of significant DEGs in RSV infected *versus* mock-treated animals
705 Table S2. Patient characteristics
706 Table S3. List of qPCR primers
707 Table S4. List of antibodies used

708 **REFERENCES**

709 1. Crisan M, Yap S, Casteilla L, Chen CW, Corselli M, Park TS, et al. A perivascular origin
710 for mesenchymal stem cells in multiple human organs. Cell stem cell. 2008;3(3):301-13. doi:
711 10.1016/j.stem.2008.07.003. PubMed PMID: 18786417.

712 2. Hennrick KT, Keeton AG, Nanua S, Kijek TG, Goldsmith AM, Sajjan US, et al. Lung cells
713 from neonates show a mesenchymal stem cell phenotype. American journal of respiratory and
714 critical care medicine. 2007;175(11):1158-64. Epub 2007/03/03. doi: 10.1164/rccm.200607-
715 941OC. PubMed PMID: 17332484.

716 3. Lama VN, Smith L, Badri L, Flint A, Andrei AC, Murray S, et al. Evidence for tissue-resident
717 mesenchymal stem cells in human adult lung from studies of transplanted allografts. J Clin Invest.
718 2007;117(4):989-96. doi: 10.1172/JCI29713. PubMed PMID: 17347686; PubMed Central PMCID:
719 PMCPMC1810571.

720 4. Jakob M, Hemeda H, Janeschik S, Bootz F, Rotter N, Lang S, et al. Human nasal mucosa
721 contains tissue-resident immunologically responsive mesenchymal stromal cells. Stem Cells Dev.
722 2010;19(5):635-44. Epub 2009/09/19. doi: 10.1089/scd.2009.0245. PubMed PMID: 19761404.

723 5. Kyu-Sup Cho H-YP, Hwan-Jung Roh, Dawn T Bravo, Peter H Hwang and Jayakar V
724 Nayak. Human ethmoid sinus mucosa: a promising novel tissue source of mesenchymal
725 progenitor cells. Stem Cell Research & Therapy. 2014.

726 6. Delorme B, Nivet E, Gaillard J, Haupl T, Ringe J, Deveze A, et al. The human nose harbors
727 a niche of olfactory ectomesenchymal stem cells displaying neurogenic and osteogenic
728 properties. Stem Cells Dev. 2010;19(6):853-66. Epub 2009/11/13. doi: 10.1089/scd.2009.0267.
729 PubMed PMID: 19905894.

730 7. Sabatini F, Petecchia L, Tavian M, Jodon de Villeroche V, Rossi GA, Brouty-Boye D.
731 Human bronchial fibroblasts exhibit a mesenchymal stem cell phenotype and multilineage
732 differentiating potentialities. Lab Invest. 2005;85(8):962-71. Epub 2005/06/01. doi:
733 10.1038/labinvest.3700300. PubMed PMID: 15924148.

734 8. Zepp JA, Zacharias WJ, Frank DB, Cavanaugh CA, Zhou S, Morley MP, et al. Distinct
735 Mesenchymal Lineages and Niches Promote Epithelial Self-Renewal and Myofibrogenesis in the
736 Lung. Cell. 2017;170(6):1134-48 e10. Epub 2017/09/09. doi: 10.1016/j.cell.2017.07.034. PubMed
737 PMID: 28886382; PubMed Central PMCID: PMCPMC5718193.

738 9. Lee JH, Tammela T, Hofree M, Choi J, Marjanovic ND, Han S, et al. Anatomically and
739 Functionally Distinct Lung Mesenchymal Populations Marked by Lgr5 and Lgr6. Cell.

740 2017;170(6):1149-63 e12. Epub 2017/09/09. doi: 10.1016/j.cell.2017.07.028. PubMed PMID:
741 28886383; PubMed Central PMCID: PMCPMC5607351.

742 10. Paris AJ, Hayer KE, Oved JH, Avgousti DC, Toulmin SA, Zepp JA, et al. STAT3-BDNF-
743 TrkB signalling promotes alveolar epithelial regeneration after lung injury. Nat Cell Biol.
744 2020;22(10):1197-210. Epub 2020/09/30. doi: 10.1038/s41556-020-0569-x. PubMed PMID:
745 32989251.

746 11. Xie T, Wang Y, Deng N, Huang G, Taghavifar F, Geng Y, et al. Single-Cell Deconvolution
747 of Fibroblast Heterogeneity in Mouse Pulmonary Fibrosis. Cell Rep. 2018;22(13):3625-40. Epub
748 2018/03/29. doi: 10.1016/j.celrep.2018.03.010. PubMed PMID: 29590628; PubMed Central
749 PMCID: PMCPMC5908225.

750 12. Beers MF, Morrisey EE. The three R's of lung health and disease: repair, remodeling, and
751 regeneration. J Clin Invest. 2011;121(6):2065-73. Epub 2011/06/03. doi: 10.1172/JCI45961.
752 PubMed PMID: 21633173; PubMed Central PMCID: PMCPMC3104764.

753 13. Aggarwal S, Pittenger MF. Human mesenchymal stem cells modulate allogeneic immune
754 cell responses. Blood. 2005;105(4):1815-22. Epub 2004/10/21. doi: 10.1182/blood-2004-04-
755 1559. PubMed PMID: 15494428.

756 14. Glassberg MK, Minkiewicz J, Toonkel RL, Simonet ES, Rubio GA, DiFede D, et al.
757 Allogeneic Human Mesenchymal Stem Cells in Patients With Idiopathic Pulmonary Fibrosis via
758 Intravenous Delivery (AETHER): A Phase I Safety Clinical Trial. Chest. 2017;151(5):971-81. Epub
759 2016/11/29. doi: 10.1016/j.chest.2016.10.061. PubMed PMID: 27890713; PubMed Central
760 PMCID: PMCPMC6026255.

761 15. Islam MN, Das SR, Emin MT, Wei M, Sun L, Westphalen K, et al. Mitochondrial transfer
762 from bone-marrow-derived stromal cells to pulmonary alveoli protects against acute lung injury.
763 Nat Med. 2012;18(5):759-65. Epub 2012/04/17. doi: 10.1038/nm.2736. PubMed PMID:
764 22504485; PubMed Central PMCID: PMCPMC3727429.

765 16. Falsey AR, Hennessey PA, Formica MA, Cox C, Walsh EE. Respiratory syncytial virus
766 infection in elderly and high-risk adults. N Engl J Med. 2005;352(17):1749-59. Epub 2005/04/29.
767 doi: 10.1056/NEJMoa043951. PubMed PMID: 15858184.

768 17. Coultas JA, Smyth R, Openshaw PJ. Respiratory syncytial virus (RSV): a scourge from
769 infancy to old age. Thorax. 2019;74(10):986-93. Epub 2019/08/07. doi: 10.1136/thoraxjnl-2018-
770 212212. PubMed PMID: 31383776.

771 18. Olivier A, Gallup J, de Macedo MM, Varga SM, Ackermann M. Human respiratory syncytial
772 virus A2 strain replicates and induces innate immune responses by respiratory epithelia of
773 neonatal lambs. Int J Exp Pathol. 2009;90(4):431-8. doi: 10.1111/j.1365-2613.2009.00643.x.
774 PubMed PMID: 19659901; PubMed Central PMCID: PMCPMC2741153.

775 19. Sitthicharoenchai P, Alnajjar S, Ackermann MR. A model of respiratory syncytial virus
776 (RSV) infection of infants in newborn lambs. Cell Tissue Res. 2020;380(2):313-24. Epub
777 2020/04/30. doi: 10.1007/s00441-020-03213-w. PubMed PMID: 32347384; PubMed Central
778 PMCID: PMCPMC7223741.

779 20. Altamirano-Lagos MJ, Diaz FE, Mansilla MA, Rivera-Perez D, Soto D, McGill JL, et al.
780 Current Animal Models for Understanding the Pathology Caused by the Respiratory Syncytial
781 Virus. Front Microbiol. 2019;10:873. Epub 2019/05/28. doi: 10.3389/fmicb.2019.00873. PubMed
782 PMID: 31130923; PubMed Central PMCID: PMCPMC6510261.

783 21. Villenave R, Thavagnanam S, Sarlang S, Parker J, Douglas I, Skibinski G, et al. In vitro
784 modeling of respiratory syncytial virus infection of pediatric bronchial epithelium, the primary
785 target of infection in vivo. Proceedings of the National Academy of Sciences of the United States
786 of America. 2012;109(13):5040-5. doi: 10.1073/pnas.1110203109. PubMed PMID: 22411804;
787 PubMed Central PMCID: PMC3323997.

788 22. Fonceca AM, Flanagan BF, Trinick R, Smyth RL, McNamara PS. Primary airway epithelial
789 cultures from children are highly permissive to respiratory syncytial virus infection. Thorax.
790 2012;67(1):42-8. Epub 2011/08/26. doi: 10.1136/thoraxjnl-2011-200131. PubMed PMID:
791 21865207.

792 23. Zhang L, Peeples ME, Boucher RC, Collins PL, Pickles RJ. Respiratory syncytial virus
793 infection of human airway epithelial cells is polarized, specific to ciliated cells, and without obvious
794 cytopathology. J Virol. 2002;76(11):5654-66. Epub 2002/05/07. doi: 10.1128/jvi.76.11.5654-
795 5666.2002. PubMed PMID: 11991994; PubMed Central PMCID: PMCPMC137037.

796 24. Dominici M, Le Blanc K, Mueller I, Slaper-Cortenbach I, Marini F, Krause D, et al. Minimal
797 criteria for defining multipotent mesenchymal stromal cells. The International Society for Cellular
798 Therapy position statement. Cytotherapy. 2006;8(4):315-7. Epub 2006/08/23. doi:
799 10.1080/14653240600855905. PubMed PMID: 16923606.

800 25. Evelyn A. Kurt-Jones LP, Laura Kwinn, Lia M. Haynes, Les P. Jones,, Ralph A.Tripp EEW,
801 Mason W. Freeman, Douglas T. Golenbock,, Finberg LJAaRW. Pattern recognition receptors
802 TLR4 and CD14 mediate response to respiratory syncytial virus. Nature Immunology. 2000;1.

803 26. Behera AK, Matsuse H, Kumar M, Kong X, Lockey RF, Mohapatra SS. Blocking
804 intercellular adhesion molecule-1 on human epithelial cells decreases respiratory syncytial virus
805 infection. Biochem Biophys Res Commun. 2001;280(1):188-95. Epub 2001/02/13. doi:
806 10.1006/bbrc.2000.4093. PubMed PMID: 11162498.

807 27. Malhotra R, Ward M, Bright H, Priest R, Foster Martyn R, Hurle M, et al. Isolation and
808 characterisation of potential respiratory syncytial virus receptor(s) on epithelial cells. Microbes
809 and Infection. 2003;5(2):123-33. doi: 10.1016/s1286-4579(02)00079-5.

810 28. Tayyari F, Marchant D, Moraes TJ, Duan W, Mastrangelo P, Hegele RG. Identification of
811 nucleolin as a cellular receptor for human respiratory syncytial virus. Nature medicine.
812 2011;17(9):1132-5. doi: 10.1038/nm.2444. PubMed PMID: 21841784.

813 29. Tripp RA, Jones LP, Haynes LM, Zheng H, Murphy PM, Anderson LJ. CX3C chemokine
814 mimicry by respiratory syncytial virus G glycoprotein. Nat Immunol. 2001;2(8):732-8. Epub
815 2001/07/31. doi: 10.1038/90675. PubMed PMID: 11477410.

816 30. Johnson SM, McNally BA, Ioannidis I, Flano E, Teng MN, Oomens AG, et al. Respiratory
817 Syncytial Virus Uses CX3CR1 as a Receptor on Primary Human Airway Epithelial Cultures. PLoS
818 pathogens. 2015;11(12):e1005318. Epub 2015/12/15. doi: 10.1371/journal.ppat.1005318.
819 PubMed PMID: 26658574; PubMed Central PMCID: PMCPMC4676609.

820 31. Schoggins JW, Rice CM. Interferon-stimulated genes and their antiviral effector functions.
821 Curr Opin Virol. 2011;1(6):519-25. Epub 2012/02/14. doi: 10.1016/j.coviro.2011.10.008. PubMed
822 PMID: 22328912; PubMed Central PMCID: PMCPMC3274382.

823 32. Bichsel CA, Wang L, Froment L, Berezowska S, Muller S, Dorn P, et al. Increased PD-L1
824 expression and IL-6 secretion characterize human lung tumor-derived perivascular-like cells that
825 promote vascular leakage in a perfusable microvasculature model. Sci Rep. 2017;7(1):10636.
826 Epub 2017/09/08. doi: 10.1038/s41598-017-09928-1. PubMed PMID: 28878242; PubMed
827 Central PMCID: PMCPMC5587684.

828 33. Klyushnenkova E, Mosca JD, Zernetkina V, Majumdar MK, Beggs KJ, Simonetti DW, et
829 al. T cell responses to allogeneic human mesenchymal stem cells: immunogenicity, tolerance,
830 and suppression. J Biomed Sci. 2005;12(1):47-57. Epub 2005/05/03. doi: 10.1007/s11373-004-
831 8183-7. PubMed PMID: 15864738.

832 34. McCarty RC, Gronthos S, Zannettino AC, Foster BK, Xian CJ. Characterisation and
833 developmental potential of ovine bone marrow derived mesenchymal stem cells. J Cell Physiol.
834 2009;219(2):324-33. doi: 10.1002/jcp.21670. PubMed PMID: 19115243.

835 35. Zhao S, Tao L, Tian Y, Tai D, Liu P, Liu D. Isolation and characterization of ovine umbilical
836 cord-derived mesenchymal stem cells. Cytotechnology. 2019;71(1):277-86. Epub 2019/01/04.
837 doi: 10.1007/s10616-018-0284-7. PubMed PMID: 30603926; PubMed Central PMCID:
838 PMCPMC6368499.

839 36. Jakub Grzesiak KM, Karol Wrzeszcz, Joanna Czogała. Isolation and Morphological
840 Characterisation of Ovine Adipose-Derived Mesenchymal Stem Cells in Culture. International
841 Journal of Stem Cells. 2011;4.

842 37. O'Connor K. A cautionary tale about the use of colony-forming efficiency as a proxy for
843 the survival of mesenchymal stem cells. Stem Cell Res Ther. 2020;11(1):292. Epub 2020/07/18.
844 doi: 10.1186/s13287-020-01805-5. PubMed PMID: 32678014.

845 38. Friedenstein AJ, Chailakhjan RK, Lalykina KS. The development of fibroblast colonies in
846 monolayer cultures of guinea-pig bone marrow and spleen cells. Cell Tissue Kinet. 1970;3(4):393-
847 403. Epub 1970/10/01. doi: 10.1111/j.1365-2184.1970.tb00347.x. PubMed PMID: 5523063.

848 39. Spadafora R, Lu J, Khetani RS, Zhang C, Iberg A, Li H, et al. Lung-Resident Mesenchymal
849 Stromal Cells Reveal Transcriptional Dynamics of Lung Development in Preterm Infants.
850 American journal of respiratory and critical care medicine. 2018;198(7):961-4. Epub 2018/05/15.
851 doi: 10.1164/rccm.201801-0024LE. PubMed PMID: 29757681; PubMed Central PMCID:
852 PMCPMC6173067.

853 40. Rohart F, Mason EA, Matigian N, Mosbergen R, Korn O, Chen T, et al. A molecular
854 classification of human mesenchymal stromal cells. PeerJ. 2016;4:e1845. Epub 2016/04/05. doi:
855 10.7717/peerj.1845. PubMed PMID: 27042394; PubMed Central PMCID: PMCPMC4811172.

856 41. Sattentau Q. Avoiding the void: cell-to-cell spread of human viruses. Nat Rev Microbiol.
857 2008;6(11):815-26. Epub 2008/10/17. doi: 10.1038/nrmicro1972. PubMed PMID: 18923409.

858 42. Wahl A, De C, Abad Fernandez M, Lenarcic EM, Xu Y, Cockrell AS, et al. Precision mouse
859 models with expanded tropism for human pathogens. Nat Biotechnol. 2019;37(10):1163-73. Epub
860 2019/08/28. doi: 10.1038/s41587-019-0225-9. PubMed PMID: 31451733; PubMed Central
861 PMCID: PMCPMC6776695.

862 43. Jain N, Kalam H, Singh L, Sharma V, Kedia S, Das P, et al. Mesenchymal stem cells offer
863 a drug-tolerant and immune-privileged niche to Mycobacterium tuberculosis. Nat Commun.
864 2020;11(1):3062. Epub 2020/06/18. doi: 10.1038/s41467-020-16877-3. PubMed PMID:
865 32546788; PubMed Central PMCID: PMCPMC7297998.

866 44. Eisenhut M. Extrapulmonary manifestations of severe respiratory syncytial virus infection-
867 -a systematic review. Crit Care. 2006;10(4):R107. Epub 2006/07/25. doi: 10.1186/cc4984.
868 PubMed PMID: 16859512; PubMed Central PMCID: PMCPMC1751022.

869 45. Rezaee F, Gibson LF, Piktel D, Othumpangat S, Piedimonte G. Respiratory syncytial virus
870 infection in human bone marrow stromal cells. Am J Respir Cell Mol Biol. 2011;45(2):277-86.
871 Epub 2010/10/26. doi: 10.1165/rcmb.2010-0121OC. PubMed PMID: 20971883; PubMed Central
872 PMCID: PMCPMC3175557.

873 46. Cheung MB, Sampayo-Escobar V, Green R, Moore ML, Mohapatra S, Mohapatra SS.
874 Respiratory Syncytial Virus-Infected Mesenchymal Stem Cells Regulate Immunity via Interferon
875 Beta and Indoleamine-2,3-Dioxygenase. PloS one. 2016;11(10):e0163709. Epub 2016/10/04.
876 doi: 10.1371/journal.pone.0163709. PubMed PMID: 27695127; PubMed Central PMCID:
877 PMCPMC5047639.

878 47. Heinonen S, Velazquez VM, Ye F, Mertz S, Acero-Bedoya S, Smith B, et al. Immune
879 profiles provide insights into respiratory syncytial virus disease severity in young children. Sci
880 Transl Med. 2020;12(540). Epub 2020/04/24. doi: 10.1126/scitranslmed.aaw0268. PubMed
881 PMID: 32321862.

882 48. Siefker DT, Vu L, You D, McBride A, Taylor R, Jones TL, et al. Respiratory Syncytial Virus
883 Disease Severity Is Associated with Distinct CD8(+) T-Cell Profiles. American journal of
884 respiratory and critical care medicine. 2020;201(3):325-34. Epub 2019/10/24. doi:
885 10.1164/rccm.201903-0588OC. PubMed PMID: 31644878; PubMed Central PMCID:
886 PMCPMC6999109.

887 49. Besteman SB, Callaghan A, Langedijk AC, Hennus MP, Meyaard L, Mokry M, et al.
888 Transcriptome of airway neutrophils reveals an interferon response in life-threatening respiratory
889 syncytial virus infection. Clin Immunol. 2020;220:108593. Epub 2020/09/14. doi:
890 10.1016/j.clim.2020.108593. PubMed PMID: 32920212.

891 50. Bradley KC, Finsterbusch K, Schnepf D, Crotta S, Llorian M, Davidson S, et al. Microbiota-
892 Driven Tonic Interferon Signals in Lung Stromal Cells Protect from Influenza Virus Infection. Cell
893 Rep. 2019;28(1):245-56 e4. Epub 2019/07/04. doi: 10.1016/j.celrep.2019.05.105. PubMed PMID:
894 31269444.

895 51. Tisoncik JR, Korth MJ, Simmons CP, Farrar J, Martin TR, Katze MG. Into the eye of the
896 cytokine storm. Microbiol Mol Biol Rev. 2012;76(1):16-32. Epub 2012/03/07. doi:
897 10.1128/mmbr.05015-11. PubMed PMID: 22390970; PubMed Central PMCID:
898 PMCPMC3294426.

899 52. McNamara PS, Flanagan BF, Hart CA, Smyth RL. Production of chemokines in the lungs
900 of infants with severe respiratory syncytial virus bronchiolitis. The Journal of infectious diseases.
901 2005;191(8):1225-32. Epub 2005/03/19. doi: 10.1086/428855. PubMed PMID: 15776367.

902 53. Rolandsson Enes S, Andersson Sjöland A, Skog I, Hansson L, Larsson H, Le Blanc K, et
903 al. MSC from fetal and adult lungs possess lung-specific properties compared to bone marrow-
904 derived MSC. Sci Rep. 2016;6:29160. Epub 2016/07/07. doi: 10.1038/srep29160. PubMed PMID:
905 27381039; PubMed Central PMCID: PMCPMC4933903.

906 54. Nordgren SNSaTM. Lung-Resident Mesenchymal Stromal Cells are Tissue-Specific
907 Regulators of Lung Homeostasis. ajp lung cellular and molecular physiology. 2020.

908 55. Kasahara Y, Tuder RM, Taraseviciene-Stewart L, Le Cras TD, Abman S, Hirth PK, et al.
909 Inhibition of VEGF receptors causes lung cell apoptosis and emphysema. J Clin Invest.
910 2000;106(11):1311-9. Epub 2000/12/06. doi: 10.1172/jci10259. PubMed PMID: 11104784;
911 PubMed Central PMCID: PMCPMC387249.

912 56. Aschner Y, Downey GP. Transforming Growth Factor-β: Master Regulator of the
913 Respiratory System in Health and Disease. American journal of respiratory cell and molecular
914 biology. 2016;54(5):647-55. Epub 2016/01/23. doi: 10.1165/rcmb.2015-0391TR. PubMed PMID:
915 26796672; PubMed Central PMCID: PMCPMC4942197.

916 57. Vaughan AE, Chapman HA. Regenerative activity of the lung after epithelial injury.
917 Biochim Biophys Acta. 2013;1832(7):922-30. Epub 2012/12/12. doi:
918 10.1016/j.bbadis.2012.11.020. PubMed PMID: 23219956.

919 58. Boregowda SV, Krishnappa V, Strivelli J, Haga CL, Booker CN, Phinney DG. Basal p53
920 expression is indispensable for mesenchymal stem cell integrity. Cell Death Differ.
921 2018;25(4):679-92. Epub 2018/01/10. doi: 10.1038/s41418-017-0004-4. PubMed PMID:
922 29311623; PubMed Central PMCID: PMCPMC5883824.

923 59. Phan SH. Genesis of the myofibroblast in lung injury and fibrosis. Proc Am Thorac Soc.
924 2012;9(3):148-52. Epub 2012/07/18. doi: 10.1513/pats.201201-011AW. PubMed PMID:
925 22802289; PubMed Central PMCID: PMCPMC5830705.

926 60. Respiratory Syncytial Virus and Recurrent Wheeze in Healthy Preterm Infants. N Engl J
927 Med. 2016;374(24):2406. Epub 2016/06/16. doi: 10.1056/NEJMx160016. PubMed PMID:
928 27305208.

929 61. Miller EK, Avila PC, Khan YW, Word CR, Pelz BJ, Papadopoulos NG, et al. Wheezing
930 exacerbations in early childhood: evaluation, treatment, and recent advances relevant to the

931 genesis of asthma. J Allergy Clin Immunol Pract. 2014;2(5):537-43. Epub 2014/09/13. doi:
932 10.1016/j.jaip.2014.06.024. PubMed PMID: 25213046; PubMed Central PMCID:
933 PMCPMC4190166.

934 62. Millar JE, Bartnikowski N, Passmore MR, Obonyo NG, Malfertheiner MV, von Bahr V, et
935 al. Combined Mesenchymal Stromal Cell Therapy and Extracorporeal Membrane Oxygenation in
936 Acute Respiratory Distress Syndrome. A Randomized Controlled Trial in Sheep. American journal
937 of respiratory and critical care medicine. 2020;202(3):383-92. Epub 2020/04/16. doi:
938 10.1164/rccm.201911-2143OC. PubMed PMID: 32293914; PubMed Central PMCID:
939 PMCPMC7397785.

940 63. Zumla A, Rao M, Wallis RS, Kaufmann SH, Rustomjee R, Mwaba P, et al. Host-directed
941 therapies for infectious diseases: current status, recent progress, and future prospects. Lancet
942 Infect Dis. 2016;16(4):e47-63. Epub 2016/04/03. doi: 10.1016/s1473-3099(16)00078-5. PubMed
943 PMID: 27036359; PubMed Central PMCID: PMCPMC7164794.

944 64. Chan MC, Kuok DI, Leung CY, Hui KP, Valkenburg SA, Lau EH, et al. Human
945 mesenchymal stromal cells reduce influenza A H5N1-associated acute lung injury in vitro and in
946 vivo. Proceedings of the National Academy of Sciences of the United States of America.
947 2016;113(13):3621-6. Epub 2016/03/16. doi: 10.1073/pnas.1601911113. PubMed PMID:
948 26976597; PubMed Central PMCID: PMCPMC4822574.

949 65. Yudhawati R, Amin M, Rantam FA, Prasetya RR, Dewantari JR, Nastri AM, et al. Bone
950 marrow-derived mesenchymal stem cells attenuate pulmonary inflammation and lung damage
951 caused by highly pathogenic avian influenza A/H5N1 virus in BALB/c mice. BMC Infect Dis.
952 2020;20(1):823. Epub 2020/11/13. doi: 10.1186/s12879-020-05525-2. PubMed PMID: 33176722;
953 PubMed Central PMCID: PMCPMC7656227.

954 66. Khoury M, Cuenca J, Cruz FF, Figueroa FE, Rocco PRM, Weiss DJ. Current status of cell-
955 based therapies for respiratory virus infections: applicability to COVID-19. The European
956 respiratory journal. 2020;55(6). Epub 2020/04/09. doi: 10.1183/13993003.00858-2020. PubMed
957 PMID: 32265310; PubMed Central PMCID: PMCPMC7144273 IT16I10084), during the conduct
958 of the study; stipend received from Cells for Cells, outside the submitted work; has patents
959 WO2014135924A1 pending, WO2017064670A2 pending, WO2017064672A1 pending and
960 WO/2019/051623 pending; and is CSO of Cells for Cells, a University spin-off developing
961 therapies for osteoarthritis, pulpitis and cardiac failure, and Regenero, a consortium for Chilean
962 regenerative medicine (public and private funding), for skin ulcer and Lupus. Conflict of interest:
963 J. Cuenca reports grants from CONICYT (FONDEF 2016, IT16I10084), during the conduct of the
964 study; stipend received from Cells for Cells, outside the submitted work; and is a research scientist
965 for Cells for Cells, a University spin-off developing therapies for osteoarthritis, pulpitis and cardiac

966 failure, and Regenero, a consortium for Chilean regenerative medicine (public and private
967 funding), for skin ulcer and Lupus. Conflict of interest: F.F. Cruz has nothing to disclose. Conflict
968 of interest: F.E. Figueroa has a patent WO/2019/051623 pending and is a board member of Cells
969 for Cells, as the director of the programme of translational cell therapy at Universidad de los
970 Andes, the academic institution that originated the Consorcio Corfo Regenero and the Cells for
971 Cells biotechnological spin-off. Conflict of interest: P.R.M. Rocco has nothing to disclose. Conflict
972 of interest: D.J. Weiss reports grants from NIH, Cystic Fibrosis Foundation and US Department
973 of Defense, outside the submitted work.

974 67. Saldanha-Araujo F, Melgaço Garcez E, Silva-Carvalho AE, Carvalho JL. Mesenchymal
975 Stem Cells: A New Piece in the Puzzle of COVID-19 Treatment. Front Immunol. 2020;11:1563.
976 Epub 2020/07/29. doi: 10.3389/fimmu.2020.01563. PubMed PMID: 32719683; PubMed Central
977 PMCID: PMCPMC7347794.

978 68. Liang B, Chen J, Li T, Wu H, Yang W, Li Y, et al. Clinical remission of a critically ill COVID-
979 19 patient treated by human umbilical cord mesenchymal stem cells: A case report. Medicine
980 (Baltimore). 2020;99(31):e21429. Epub 2020/08/07. doi: 10.1097/md.0000000000021429.
981 PubMed PMID: 32756149; PubMed Central PMCID: PMCPMC7402800.

982 69. Guo Z, Chen Y, Luo X, He X, Zhang Y, Wang J. Administration of umbilical cord
983 mesenchymal stem cells in patients with severe COVID-19 pneumonia. Crit Care.
984 2020;24(1):420. Epub 2020/07/13. doi: 10.1186/s13054-020-03142-8. PubMed PMID: 32653043;
985 PubMed Central PMCID: PMCPMC7351637.

986 70. Thanunchai M, Hongeng S, Thitithanyanont A. Mesenchymal Stromal Cells and Viral
987 Infection. Stem Cells Int. 2015;2015:860950. Epub 2015/08/22. doi: 10.1155/2015/860950.
988 PubMed PMID: 26294919; PubMed Central PMCID: PMCPMC4532961.

989 71. Scheerlinck JP, Snibson KJ, Bowles VM, Sutton P. Biomedical applications of sheep
990 models: from asthma to vaccines. Trends Biotechnol. 2008;26(5):259-66. Epub 2008/03/21. doi:
991 10.1016/j.tibtech.2008.02.002. PubMed PMID: 18353472.

992 72. Wang L, Dorn P, Zeinali S, Froment L, Berezowska S, Kocher GJ, et al. CD90+CD146+
993 identifies a pulmonary mesenchymal cell subtype with both immune modulatory and perivascular-
994 like function in postnatal human lung. Am J Physiol Lung Cell Mol Physiol. 2020. doi:
995 10.1152/ajplung.00146.2019.

996 73. Rameix-Welti MA, Le Goffic R, Hervé PL, Sourimant J, Rémot A, Riffault S, et al.
997 Visualizing the replication of respiratory syncytial virus in cells and in living mice. Nat Commun.
998 2014;5:5104. Epub 2014/10/04. doi: 10.1038/ncomms6104. PubMed PMID: 25277263; PubMed
999 Central PMCID: PMCPMC7091779.

1000 74. Hallak LK, Spillmann D, Collins PL, Peeples ME. Glycosaminoglycan sulfation
1001 requirements for respiratory syncytial virus infection. J Virol. 2000;74(22):10508-13. Epub
1002 2000/10/24. doi: 10.1128/jvi.74.22.10508-10513.2000. PubMed PMID: 11044095; PubMed
1003 Central PMCID: PMCPMC110925.

1004 75. Blockus S, Sake SM, Wetzke M, Grethe C, Graalmann T, Pils M, et al. Labyrinthopeptins
1005 as virolytic inhibitors of respiratory syncytial virus cell entry. Antiviral Res. 2020;177:104774. Epub
1006 2020/03/22. doi: 10.1016/j.antiviral.2020.104774. PubMed PMID: 32197980.

1007 76. Alves MP, Neuhaus V, Guzylack-Piriou L, Ruggli N, McCullough KC, Summerfield A. Toll-
1008 like receptor 7 and MyD88 knockdown by lentivirus-mediated RNA interference to porcine
1009 dendritic cell subsets. Gene Ther. 2007;14(10):836-44. PubMed PMID: 17330086.

1010 77. Mehinagic K, Pilo P, Vidondo B, Stokar-Regenscheit N. Coinfection of Swiss cattle with
1011 bovine parainfluenza virus 3 and Mycoplasma bovis at acute and chronic stages of bovine
1012 respiratory disease complex. J Vet Diagn Invest. 2019;31(5):674-80. Epub 2019/06/28. doi:
1013 10.1177/1040638719861686. PubMed PMID: 31246162; PubMed Central PMCID:
1014 PMCPMC6727125.

1015 78. Auray G, Keller I, Python S, Gerber M, Bruggmann R, Ruggli N, et al. Characterization
1016 and Transcriptomic Analysis of Porcine Blood Conventional and Plasmacytoid Dendritic Cells
1017 Reveals Striking Species-Specific Differences. J Immunol. 2016;197(12):4791-806. Epub
1018 2016/11/12. doi: 10.4049/jimmunol.1600672. PubMed PMID: 27837108.

1019 79. Wang L, Wang S, Li W. RSeQC: quality control of RNA-seq experiments. Bioinformatics.
1020 2012;28(16):2184-5. Epub 2012/06/30. doi: 10.1093/bioinformatics/bts356. PubMed PMID:
1021 22743226.

1022 80. Kim D, Langmead B, Salzberg SL. HISAT: a fast spliced aligner with low memory
1023 requirements. Nat Methods. 2015;12(4):357-60. Epub 2015/03/10. doi: 10.1038/nmeth.3317.
1024 PubMed PMID: 25751142; PubMed Central PMCID: PMCPMC4655817.

1025 81. Liao Y, Smyth GK, Shi W. featureCounts: an efficient general purpose program for
1026 assigning sequence reads to genomic features. Bioinformatics. 2014;30(7):923-30. Epub
1027 2013/11/15. doi: 10.1093/bioinformatics/btt656. PubMed PMID: 24227677.

1028 82. Love MI, Huber W, Anders S. Moderated estimation of fold change and dispersion for
1029 RNA-seq data with DESeq2. Genome Biol. 2014;15(12):550. Epub 2014/12/18. doi:
1030 10.1186/s13059-014-0550-8. PubMed PMID: 25516281; PubMed Central PMCID:
1031 PMCPMC4302049.

1032 83. Wagner GP, Kin K, Lynch VJ. Measurement of mRNA abundance using RNA-seq data:
1033 RPKM measure is inconsistent among samples. Theory Biosci. 2012;131(4):281-5. Epub
1034 2012/08/09. doi: 10.1007/s12064-012-0162-3. PubMed PMID: 22872506.

1035 84. Liberzon A, Birger C, Thorvaldsdóttir H, Ghandi M, Mesirov JP, Tamayo P. The Molecular
1036 Signatures Database (MSigDB) hallmark gene set collection. Cell Syst. 2015;1(6):417-25. Epub
1037 2016/01/16. doi: 10.1016/j.cels.2015.12.004. PubMed PMID: 26771021; PubMed Central
1038 PMCID: PMCPMC4707969.
1039

1040

1041 **FIGURE LEGENDS**

1042 **Figure 1**: **LR-MSCs are highly permissive to RSV infection**

1043 (A) Representative histograms showing expression of the surface markers CD73, CD90, CD105
1044 on pediatric LR-MSCs. (B) Representative phase-contrast (PC) micrograph showing morphology
1045 in culture and demonstrates plastic adherence. Representative images of Toluidine blue, Alizarin
1046 Red S, and Oil Red O stainings after chondrogenic (C), osteogenic (O), and adipogenic (A)
1047 differentiation, respectively. Magnification 40X (PC, O) and 200X (C, A). (C) mRNA expression
1048 levels of RSV receptors relative to 10^6 18S. A Mann-Whitney U test was applied to compare the
1049 two cell types (AECs *versus* LR-MSCs). Boxplots indicate the median value (centerline) and
1050 interquartile ranges (box edges), with whiskers extending to the lowest and the highest values.
1051 Each symbol represents an individual donor (n=5). *$p<0.05$, **$p<0.01$. (D) Intracellular viral loads
1052 in AECs and LR-MSCs over time following infection with RSV-A2 at a MOI of 1 PFU/cell
1053 expressed as RSV copies per 10^{12} 18S copies. Each symbol represents an individual donor (n=5).
1054 (E) RSV F-protein positive LR-MSCs assessed by FCM and plotted over time. LR-MSCs were
1055 infected with 0.1 PFU/cell with RSV-A2 (n=3) or a clinical isolate RSV-ON1-H1 (n=4-6). Each
1056 symbol represents an individual donor. (F) Representative live-cell imaging of WD-AECs and LR-
1057 MSCs infected with 0.1-0.5 PFU/cell with RSV-mCherry and followed over time. The micrographs
1058 were taken at 16, 32, and 48 h p.i. in the same area of the cellular layer. (G) Representative
1059 confocal microscopy evaluation of LR-MSCs noninfected (mock) or infected with RSV-A2 at 1
1060 PFU/cell 24 to 72 hours p.i. RSV, green; DAPI, dark blue; WGA, white. Scale bar, 20 µm. (H)
1061 Supernatants of infected LR-MSCs or apical washes of infected WD-AEC cultures were analyzed
1062 by a PFU assay. Cells were infected with RSV-ON1-H1 at a MOI of 0.1 PFU/cell. A Mann-Whitney
1063 U test was applied to compare the two cell types (WD-AECs, n=3 *versus* LR-MSCs, n=5-6). Each
1064 symbol represents an individual donor. *$p<0.05$, **$p<0.01$. (I) Intracellular infectious RSV titers in
1065 LR-MSCs infected with RSV-A2 or RSV-ON1-H1 at 0.1 PFU/cell. Each symbol represents an
1066 individual donor (n=3) (J). Extracellular RSV RNA load over time in supernatants of infected LR-
1067 MSCs or apical washes of infected WD-AEC cultures. Cells were infected with RSV-ON1-H1 at a

1068 MOI of 0.1 PFU/cell. A Mann-Whitney U test was applied to compare the two cell types (WD-
1069 AECs, n=3 *versus* LR-MSCs, n=4-6). Each symbol represents an individual donor. *p<0.05.
1070
1071 **Figure 2: RSV infection is altering the immune properties of LR-MSCs**
1072 (A, B) mRNA levels of selected ISGs (A) and IFNs (B) in LR-MSCs treated with mock control,
1073 poly(I:C) 10 μg/ml, RSV-A2, or RSV-ON1-H1 for 24 h at 1 PFU/cell. Boxplots indicate the median
1074 value (centerline) and interquartile ranges (box edges), with whiskers extending to the lowest and
1075 the highest values. Each symbol represents an individual donor (mock, n=6; poly(I:C), n=5; RSV-
1076 A2, n=4; RSV-ON1-H1, n=6). The data were compared with the Kruskal–Wallis test followed by
1077 Dunn's post hoc test. *p<0.05, **p<0.01. (C, D) IFN-β (C) and IFN-λ1/3 (D) protein levels in
1078 supernatants of LR-MSCs treated with mock control, poly(I:C) 10 μg/ml, RSV-A2, or RSV-ON1-
1079 H1 for 24 h and 72 h at 1 PFU/cell. Boxplots indicate median value (centerline) and interquartile
1080 ranges (box edges), with whiskers extending to the lowest and the highest values. Each symbol
1081 represents an individual donor (mock, n=6; poly(I:C), n=5; RSV-A2, n=4; RSV-ON1-H1, n=6). A
1082 Kruskal–Wallis test followed by a Dunn's post hoc test was applied to compare the different
1083 groups. *p<0.05, **p<0.01, ***p<0.001. The detection limits of the assays are indicated with the
1084 dotted line at 7.7 pg/mL and 79.8 pg/mL for IFN-β and IFN-λ1/3, respectively. (E, F) Multiplex
1085 assay of supernatants of LR-MSCs (E) or basolateral medium of WD-AECs (F), 24 and 72h after
1086 treatment with mock control, 10 μg/ml poly(I:C), RSV-A2, or RSV-ON1-H1 for 24h and 72h at 1
1087 PFU/cell. The concentration ranges of the different cytokines are indicated (lower detection limit-
1088 highest concentration measured). An asterisk is present when the concentration of the sample
1089 was higher than the upper range of the assay. Each column represents a different donor (mock,
1090 n=6; poly(I:C), n=5; RSV-A2, n=4; RSV-ON1-H1, n=6). (donors a-c for WD-AECs and d-i for LR-
1091 MSCs). (G) Overview of the impact of RSV infection of LR-MSCs activity. RSV-mediated
1092 activation of LR-MSCs, characterized by an antiviral and pro-inflammatory phenotype combined
1093 with cytokines promoting T helper cell (Th) polarization.
1094

1095 **Figure 3**: **RSV infection is causing lung injury in lamb**

1096 (A) Newborn animals were trans-tracheal inoculated with 10^8 PFU per animal of the human strain
1097 RSV-A2 or PBS (mock). Animals were euthanized 3, 6, 14, and 42 days p.i. and lung and BAL
1098 tissues were harvested for histopathological evaluation, qPCR, and FCM analysis (B)
1099 Representative H&E stained histopathological sections of the lung tissue from noninfected (mock)
1100 and RSV-infected lambs at 3, 6, 14, and 42 days p.i. Scale bar, 200 µm. (C) Histological lung
1101 sections from animals 6 days p.i. stained for RSV (red) and counterstained with haematoxylin
1102 (blue). From left to right panels, scale bars 50 µm, 100 µm and 20 µm, respectively. (D) Viral load
1103 in lungs and the cellular fraction of the BAL of infected lambs measured 3, 6, 14, and 42 days p.i.
1104 Comparison of viral loads between BAL and lung tissues was done with a one-way ANOVA and
1105 the Tukey post-hoc test. Each symbol represents an individual animal (n=6 per timepoint).
1106 *$p<0.05$. (E, F) Frequency of cleaved caspase 3 (CASP3)-positive cells in the lung (E) and BAL
1107 (F) of infected animals 3 to 42 days p.i. Boxplots indicate the median value (centerline) and
1108 interquartile ranges (box edges), with whiskers extending to the lowest and the highest values.
1109 Each symbol represents an individual animal (mock, n=3 and RSV, n=6). Multiple comparison
1110 was done with a one-way ANOVA and the Tukey post-hoc test. *$p<0.05$. (G) Total BAL cell counts
1111 in mock and RSV-infected animals 3, 6, and 14 days p.i. pooled. Boxplots indicate the median
1112 value (centerline) and interquartile ranges (box edges), with whiskers extending to the lowest and
1113 the highest values. Each symbol represents an individual animal (n=9, mock and n=18, RSV). A
1114 Mann-Whitney U test was applied to compare the two groups. **$p<0.01$.

1115

1116 **Figure 4**: **LR-MSCs are a target for RSV infection *in vivo***

1117 (A) FCM gating strategy to identify RSV-infected epithelial cells ($CD31^-CD45^-panCTK^+$) (panCTK,
1118 pan-cytokeratin) and LR-MSCs ($CD31^-CD45^-panCTK^-CD29^+CD44^+$). (G1, gate 1) (B) Percentage
1119 of animals with RSV-positive epithelial and LR-MSCs 3 to 42 days p.i. The fractions indicate the
1120 number of infected animals where infection was detected by FCM compared to the total number
1121 of animals. (C) Correlation of RSV-positive LR-MSCs and RSV-positive epithelial cells at 3 and 6
1122 days p.i. Associations were tested using the Spearman rank correlation test. Each symbol

1123 represents an individual animal. (D) RSV loads in MSCs isolated from lung and BAL tissues of
1124 RSV-infected animals 3, 6, 14, and 42 d p.i. and expanded in culture. Each symbol represents an
1125 individual animal (n=6-8). (E) Phase-contrast micrographs of LR-MSCs derived from BALs
1126 expanded in culture from noninfected (mock) or infected (RSV) animals 3 days p.i. Magnification
1127 100X. The yellow arrowheads indicate a cluster of nuclei of a potential syncytium. (F)
1128 Representative confocal microscopy evaluation of LR-MSCs derived from BALs expanded in
1129 culture from noninfected (mock) or infected (RSV) animals 3 days p.i. RSV, orange; DAPI, dark
1130 blue; WGA, light blue. Scale bars, 15 µm (left and middle panels) and 10 µm for the 3D capture
1131 (right panels).
1132
1133 **Figure 5: RSV infection leads to the expansion of the pulmonary MSC niche *in vivo***
1134 (A) Newborn or adult (average age of 29 months) animals were trans-tracheal inoculated with 10^8
1135 PFU per animal of the human strain RSV-A2 or PBS (mock). Newborns were euthanized 3, 6, 14,
1136 and 42 days p.i. and adults 6 and 14 days p.i. and lung tissue was harvested for CFU-F assay.
1137 Lung tissue of adults was harvested for histopathological evaluation (B) Representative H&E
1138 stained histopathological sections of the lung tissue from noninfected (mock) and RSV-infected
1139 adults at 6 and 14 days p.i. scale bar, 200 µm. (C, E) Representative images of the CFU-F assay
1140 for mock control and RSV-infected neonates (C) and adults (E) 3 to 42 days p.i. and 6 and 14
1141 days p.i., respectively. Each image represents an individual animal. (D, F) Quantification of the
1142 CFU-F assay for each neonate (D) and adult (F) animals, given as CFU-F count relative to
1143 $3.33X10^5$ nucleated cells over time. Boxplots indicate the median value (centerline) and
1144 interquartile ranges (box edges), with whiskers extending to the lowest and the highest values.
1145 Each symbol represents an individual animal (neonates, per timepoint: mock, n=3-4; RSV, n=6-
1146 8; adults: mock, n=14; RSV, n=3 per timepoint). A one-way ANOVA and the Holm-Sydak post-
1147 hoc test was applied to compare differences between groups. *$p<0.05$, ***$p<0.001$, ****$p<0.0001$.
1148
1149 **Figure 6: The transcriptional activity of LR-MSCs is related to the phases of RSV disease**

1150 (A) Expression levels of selected classical MSC markers expressed as log_2TPM (TPM, transcripts
1151 per million). Each column is a different time p.i. (6, 14, and 42 days p.i.). (B-D) Volcano plot of the
1152 DEGs from the comparison of RSV infection and mock control 6 (B), 14 (C), and 42 (D) days p.i.
1153 with $p_{adj}<0.05$ (red filed circles). (B) Pie chart with the 14 DEGs ($p_{adj}<0.05$) categorized according
1154 to their function. (D) Pie chart with the 43 DEGs ($p_{adj}<0.05$) categorized according to their function.
1155 (E) Normalized enrichment score of significant (false discovery rate, FDR<0.05) hallmark gene
1156 sets for the comparisons of RSV infection and mock control 6, 14, and 42 days p.i.
1157 (downregulated, blue and upregulated, red) (F) Cartoon summarizing the different functions of
1158 LR-MSCs during distinct steps of RSV disease.

Fig. 1

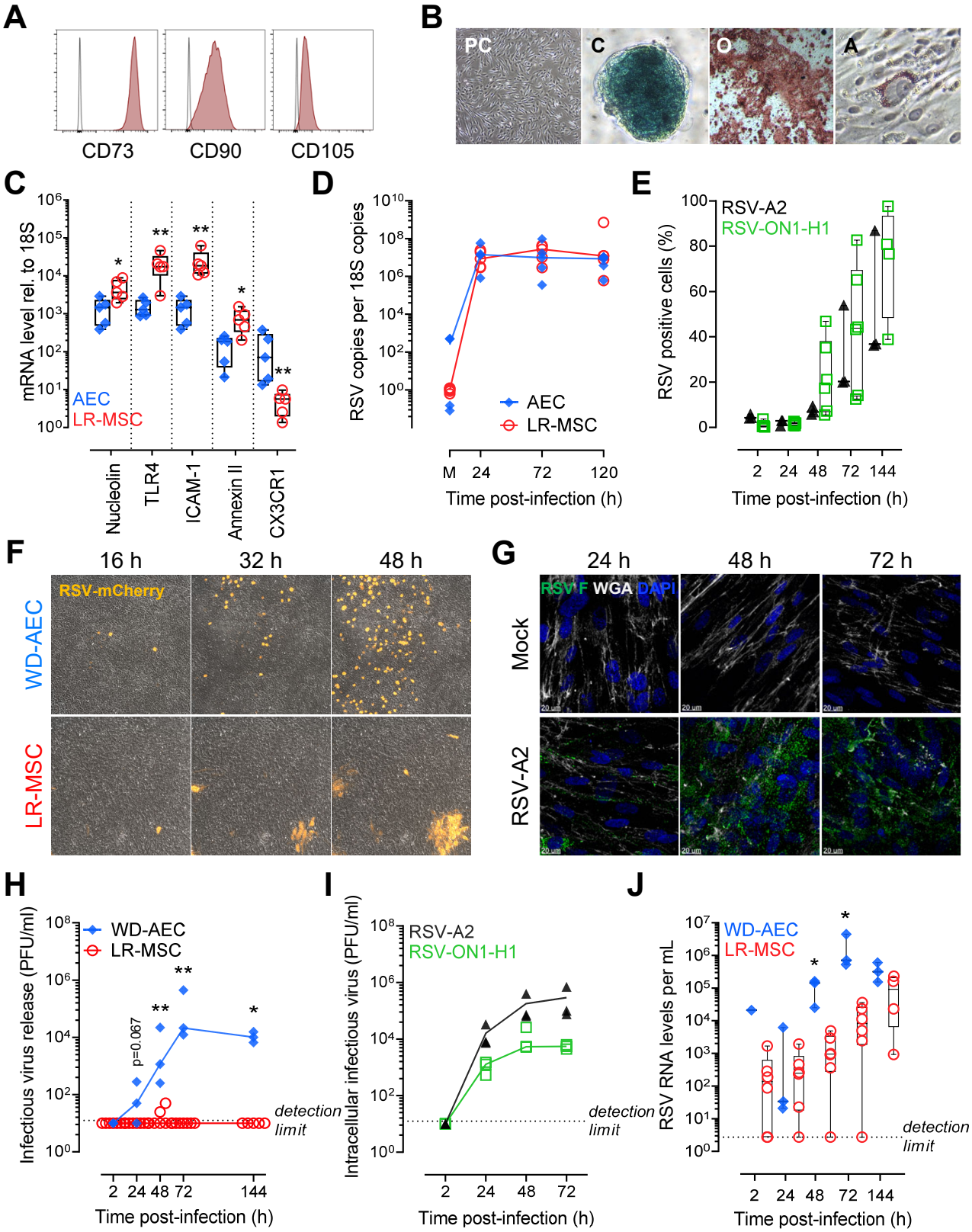
A
CD73
CD90
CD105
B
PC
C
O
A
C
mRNA level rel. to 18S
AEC
LR-MSC
Nucleolin
TLR4
ICAM-1
Annexin II
CX3CR1
D
RSV copies per 18S copies
AEC
LR-MSC
M
24
72
120
Time post-infection (h)
E
RSV positive cells (%)
RSV-A2
RSV-ON1-H1
2
24
48
72
144
Time post-infection (h)
F
16 h
32 h
48 h
RSV-mCherry
WD-AEC
LR-MSC
G
24 h
48 h
72 h
RSV F WGA DAPI
Mock
RSV-A2
H
Infectious virus release (PFU/ml)
WD-AEC
LR-MSC
p=0.067
detection limit
Time post-infection (h)
I
Intracellular infectious virus (PFU/ml)
RSV-A2
RSV-ON1-H1
detection limit
Time post-infection (h)
J
RSV RNA levels per mL
WD-AEC
LR-MSC
detection limit
Time post-infection (h)

Fig. 2

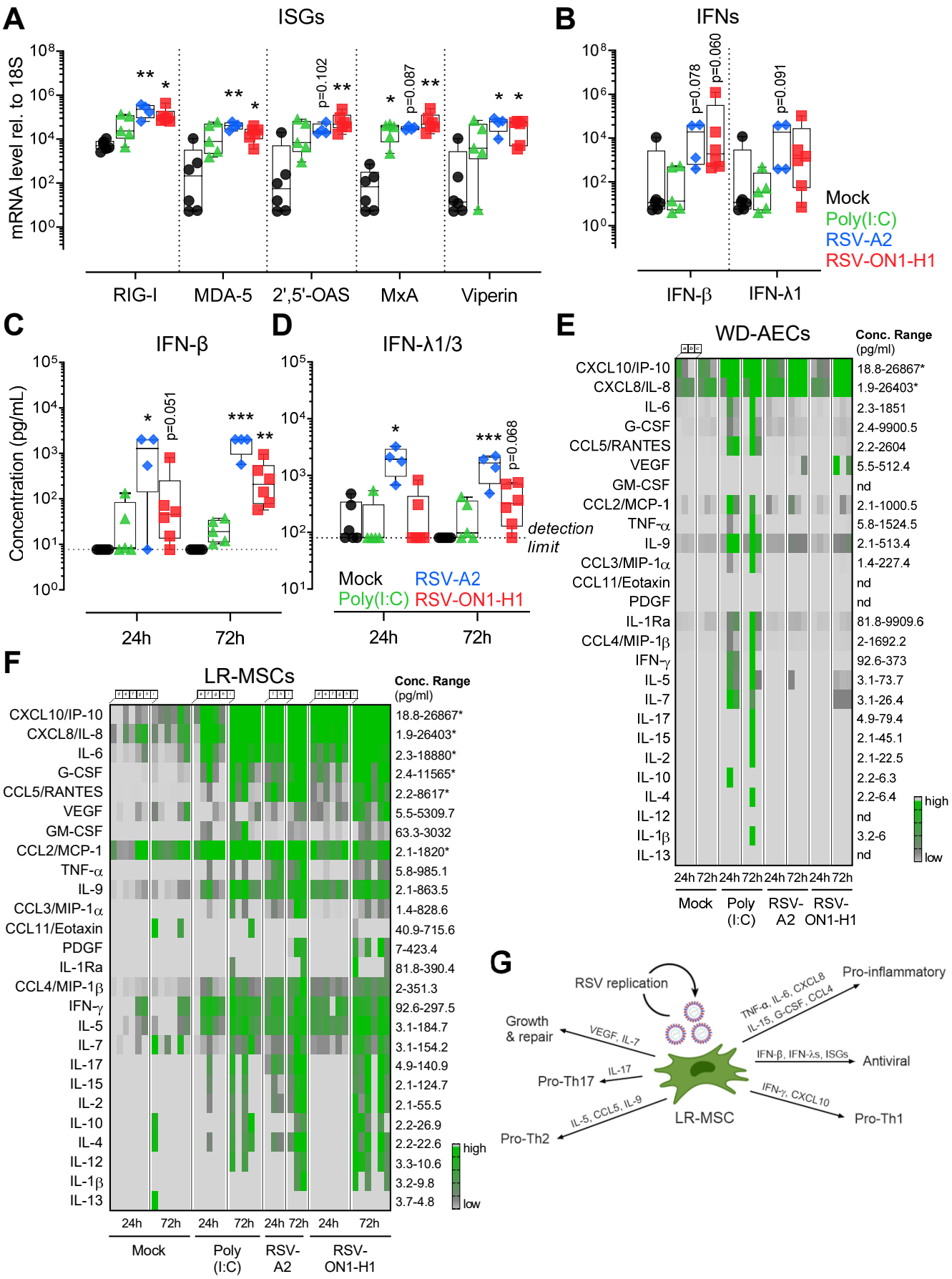
A
ISGs
mRNA level rel. to 18S
RIG-I
MDA-5
2',5'-OAS
MxA
Viperin
p=0.102
p=0.087
B
IFNs
p=0.078
p=0.060
p=0.091
IFN-β
IFN-λ1
Mock
Poly(I:C)
RSV-A2
RSV-ON1-H1
C
IFN-β
Concentration (pg/mL)
p=0.051
24h
72h
D
IFN-λ1/3
detection limit
p=0.068
E
WD-AECs
Conc. Range (pg/ml)
CXCL10/IP-10 18.8-26867*
CXCL8/IL-8 1.9-26403*
IL-6 2.3-1851
G-CSF 2.4-9900.5
CCL5/RANTES 2.2-2604
VEGF 5.5-512.4
GM-CSF nd
CCL2/MCP-1 2.1-1000.5
TNF-α 5.8-1524.5
IL-9 2.1-513.4
CCL3/MIP-1α 1.4-227.4
CCL11/Eotaxin nd
PDGF nd
IL-1Ra 81.8-9909.6
CCL4/MIP-1β 2-1692.2
IFN-γ 92.6-373
IL-5 3.1-73.7
IL-7 3.1-26.4
IL-17 4.9-79.4
IL-15 2.1-45.1
IL-2 2.1-22.5
IL-10 2.2-6.3
IL-4 2.2-6.4
IL-12 nd
IL-1β 3.2-6
IL-13 nd
high
low
Mock
Poly (I:C)
RSV-A2
RSV-ON1-H1
F
LR-MSCs
Conc. Range (pg/ml)
CXCL10/IP-10 18.8-26867*
CXCL8/IL-8 1.9-26403*
IL-6 2.3-18880*
G-CSF 2.4-11565*
CCL5/RANTES 2.2-8617*
VEGF 5.5-5309.7
GM-CSF 63.3-3032
CCL2/MCP-1 2.1-1820*
TNF-α 5.8-985.1
IL-9 2.1-863.5
CCL3/MIP-1α 1.4-828.6
CCL11/Eotaxin 40.9-715.6
PDGF 7-423.4
IL-1Ra 81.8-390.4
CCL4/MIP-1β 2-351.3
IFN-γ 92.6-297.5
IL-5 3.1-184.7
IL-7 3.1-154.2
IL-17 4.9-140.9
IL-15 2.1-124.7
IL-2 2.1-55.5
IL-10 2.2-26.9
IL-4 2.2-22.6
IL-12 3.3-10.6
IL-1β 3.2-9.8
IL-13 3.7-4.8
high
low
Mock
Poly (I:C)
RSV-A2
RSV-ON1-H1
G
RSV replication
Growth & repair
VEGF, IL-7
Pro-inflammatory
TNF-α, IL-6, CXCL8 IL-15, G-CSF, CCL4
IFN-β, IFN-λs, ISGs
Antiviral
Pro-Th17
IL-17
IFN-γ, CXCL10
Pro-Th1
IL-5, CCL5, IL-9
Pro-Th2
LR-MSC

Fig. 3

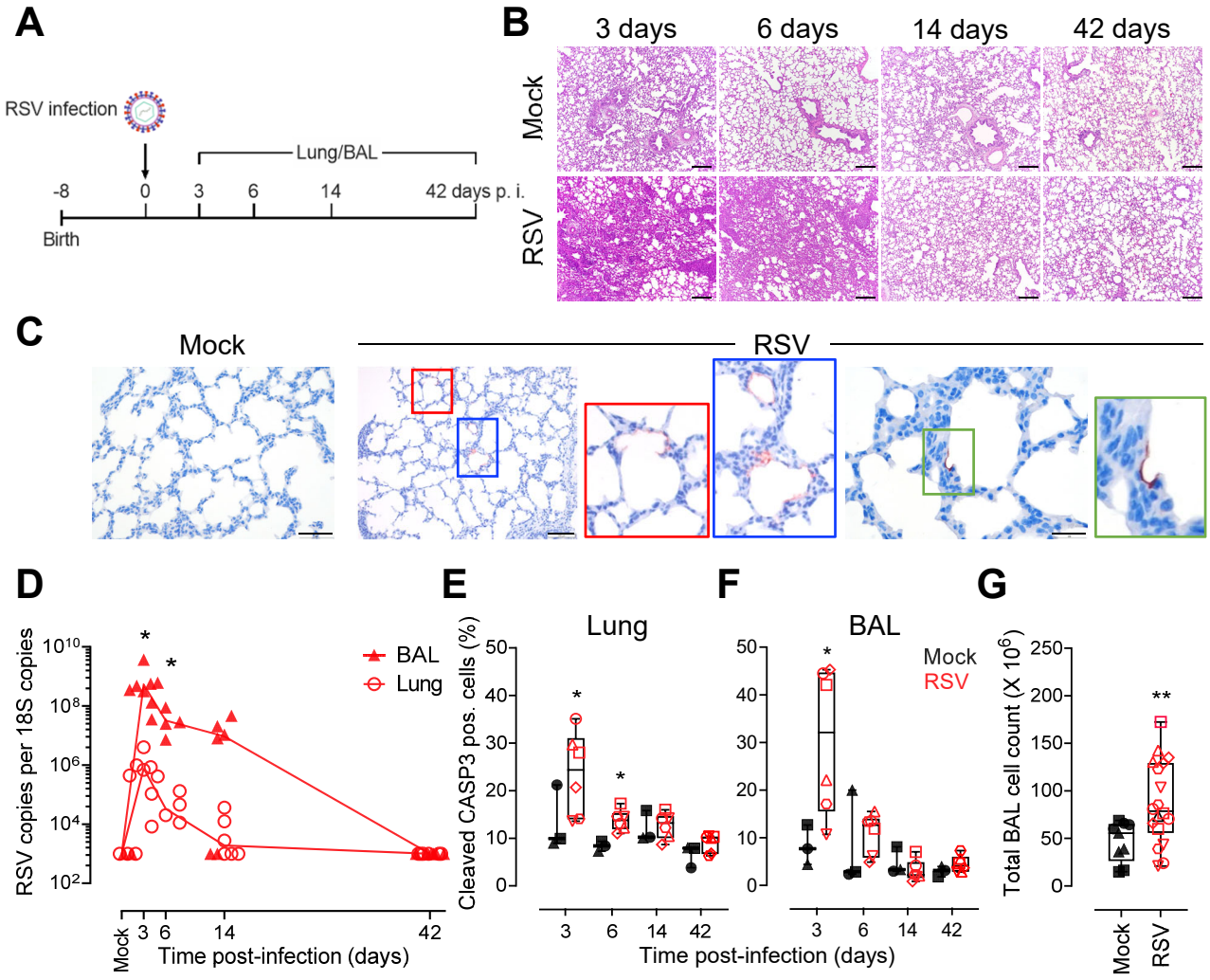
A
RSV infection
Lung/BAL
-8
0
3
6
14
42 days p. i.
Birth
B
3 days
6 days
14 days
42 days
Mock
RSV
C
Mock
RSV
D
RSV copies per 18S copies
BAL
Lung
Mock
Time post-infection (days)
E
Lung
Cleaved CASP3 pos. cells (%)
Time post-infection (days)
F
BAL
Mock
RSV
Time post-infection (days)
G
Total BAL cell count (X 10^6)
Mock
RSV

Fig. 4

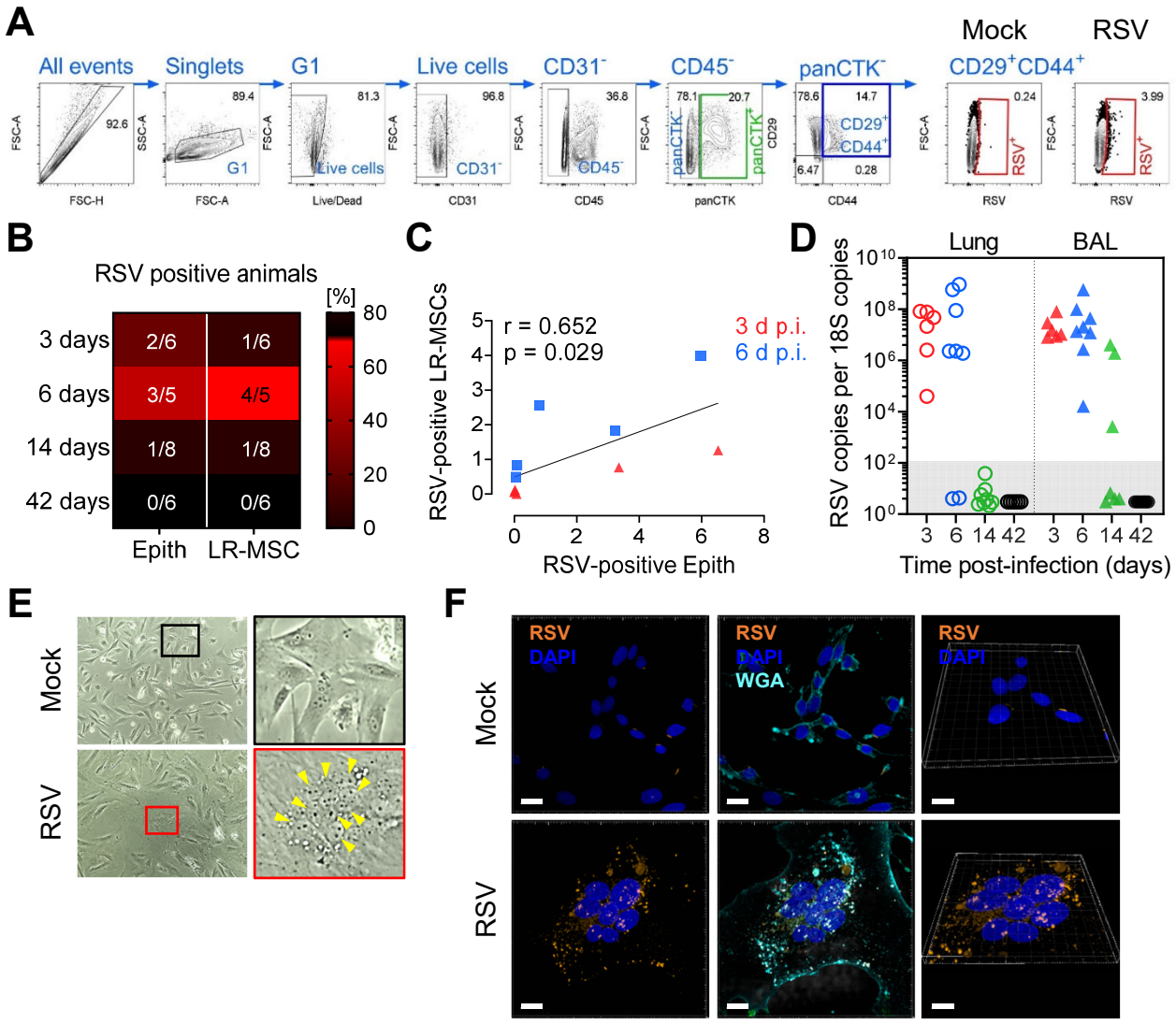
A
All events
Singlets
G1
Live cells
CD31⁻
CD45⁻
panCTK⁻
Mock
RSV
CD29⁺CD44⁺
FSC-H
FSC-A
SSC-A
Live/Dead
CD31
CD45
panCTK
CD44
CD29
RSV
B
RSV positive animals
3 days
6 days
14 days
42 days
Epith
LR-MSC
[%]
C
r = 0.652
p = 0.029
3 d p.i.
6 d p.i.
RSV-positive LR-MSCs
RSV-positive Epith
D
Lung
BAL
RSV copies per 18S copies
Time post-infection (days)
E
Mock
RSV
F
RSV
DAPI
WGA

Fig. 5

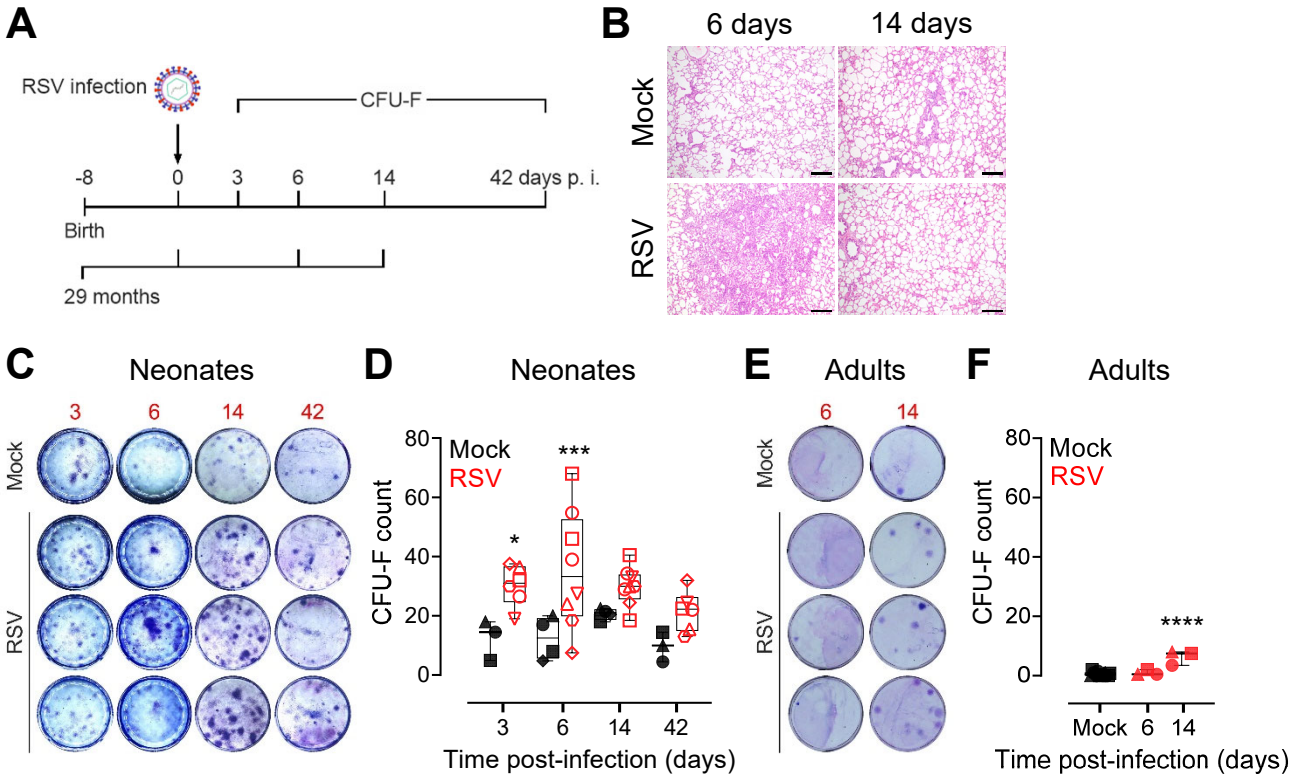
A
RSV infection
CFU-F
-8
0
3
6
14
42 days p. i.
Birth
29 months
B
6 days
14 days
Mock
RSV
C
Neonates
3
6
14
42
Mock
RSV
D
Neonates
Mock
RSV
CFU-F count
80
60
40
20
0
*
***
3
6
14
42
Time post-infection (days)
E
Adults
6
14
Mock
RSV
F
Adults
Mock
RSV
CFU-F count
80
60
40
20
0
****
Mock
6
14
Time post-infection (days)

Fig. 6

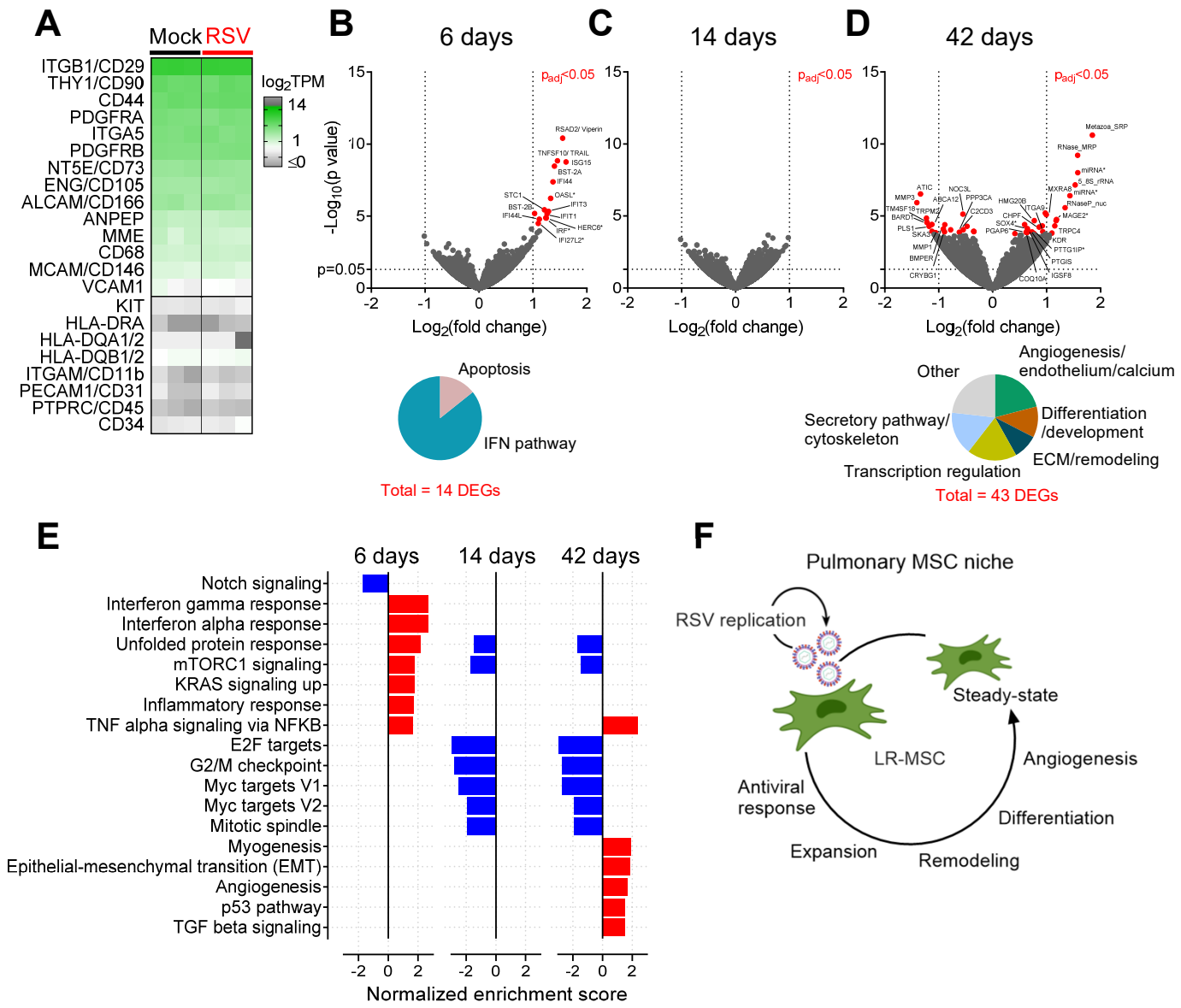
A
Mock
RSV
ITGB1/CD29
THY1/CD90
CD44
PDGFRA
ITGA5
PDGFRB
NT5E/CD73
ENG/CD105
ALCAM/CD166
ANPEP
MME
CD68
MCAM/CD146
VCAM1
KIT
HLA-DRA
HLA-DQA1/2
HLA-DQB1/2
ITGAM/CD11b
PECAM1/CD31
PTPRC/CD45
CD34
log2TPM
14
1
≤0
B
6 days
C
14 days
D
42 days
padj<0.05
-Log10(p value)
p=0.05
Log2(fold change)
Apoptosis
IFN pathway
Total = 14 DEGs
Other
Angiogenesis/
endothelium/calcium
Secretory pathway/
cytoskeleton
Differentiation
/development
ECM/remodeling
Transcription regulation
Total = 43 DEGs
E
6 days
14 days
42 days
Notch signaling
Interferon gamma response
Interferon alpha response
Unfolded protein response
mTORC1 signaling
KRAS signaling up
Inflammatory response
TNF alpha signaling via NFKB
E2F targets
G2/M checkpoint
Myc targets V1
Myc targets V2
Mitotic spindle
Myogenesis
Epithelial-mesenchymal transition (EMT)
Angiogenesis
p53 pathway
TGF beta signaling
Normalized enrichment score
F
Pulmonary MSC niche
RSV replication
Steady-state
LR-MSC
Angiogenesis
Antiviral
response
Differentiation
Expansion
Remodeling